

DesignCon 2011

Developing Unified Methods of 3D
Electromagnetic Extraction, System
Level Channel Modeling, and Robust
Jitter Decomposition in Crosstalk
Stressed 10Gbps Serial Data
Systems

13-WA1

James Bell, Wild River Technology
jim@wildrivertech.com

Scott McMorrow, Teraspeed Consulting Group
scott@teraspeed.com, +1- (401) 284-1827

Martin Miller, LeCroy Corp.
Marty.Miller@lecroy.com +1- (845) 425-2000

Alfred Neves, Wild River Technology
al@wildrivertech.com, + 1-503-718-7172

Yuriy Shlepnev, Simberian Inc.
shlepnev@simberian.com, +1-702-876-2882

Abstract

As serial link speeds increase, systems become more “Stressed”. Loss, low probability deterministic jitter, crosstalk aggression from densely packed signal nets, via and connector impedance and associated resonances, and package and power delivery issues all add their own jitter density function, resulting in a net jitter picture that is inherently complicated. This paper represents a rigorous and practical crosstalk analysis of 10Gbps and higher serial data transmission systems, which will begin at pre-layout 3D EM extraction, continue with the material parameters identification and post-layout analysis and end with direct jitter measurement and separation. We believe this is one of the timeliest of topics in signal integrity at the present time.

Authors’ Biographies

James Bell, Founder – Engineer, Wild River Technology LLC. James is an experienced design and signal integrity engineer with 30 years experience in complex system design, interconnect, and signal integrity engineering. He has been a consultant to engineering organizations world-wide, with expertise in pre- and post-route signal integrity and timing validation for advanced systems. He earned his B.S. in Electrical Engineering at Northern Arizona University. Jim can be contacted at jim@wildrivertech.com.

Scott McMorrow, President and Founder, Teraspeed Consulting Group. Mr. McMorrow is an experienced technologist with over 20 years of broad background in complex system design, interconnect & Signal Integrity engineering, modeling & measurement methodology, engineering team building and professional training. Mr. McMorrow has a consistent history of delivering and managing technical consultation that enables clients to manufacture systems with state-of-the-art performance, enhanced design margins, lower cost, and reduced risk. Mr McMorrow is an expert in high-performance design and signal integrity engineering, and has been a consultant and trainer to engineering organizations world-wide.

Martin Miller Ph.D., Chief Scientist, LeCroy Corporation. Marty received a doctorate in particle physics from the University of Rochester. He has 33 years of experience at LeCroy Corporation in various R&D functions, including analog, digital and software design. Marty has spent the past 20 years focusing on algorithms and methods for display and measurements in digital oscilloscopes, most significantly in the area of signal integrity (jitter and timing). Presently he has more than a dozen U.S. patents in this domain.

Alfred P. Neves, Founder-Engineer, Wild River Technology LLC. Al has 30 years of experience in the design and application development of semiconductor products, capital equipment design focused on jitter and signal integrity analysis, and has successfully been involved with numerous business developments and startup activity for the last 13 years. Al is involved with the Signal Integrity community as a consultant, high-speed system level design manager and engineer. Recent technical accomplishments include development of platforms and methods to improve 3D electromagnetic correspondence to

measure-based methods, including advancing time and frequency domain calibration methods. Al focuses on measure-based model development, package characterization, high-speed board design, low jitter design, analysis, and training. He earned a B.S. in Applied Mathematics at the University of Massachusetts. Al can be contacted at al@wldrivertech.com.

Yuriy Shlepnev, President and Founder, Simberian Inc., Yuriy develops Simbeor electromagnetic signal integrity software. He received an M.S. degree in radio engineering from Novosibirsk State Technical University in 1983, and a Ph.D. degree in computational electromagnetics from Siberian State University of Telecommunications and Informatics in 1990. He was principal developer of electromagnetic simulator for Eagleware Corporation and leading developer of electromagnetic software for simulation of high-speed digital circuits at Mentor Graphics. The results of his research are published in multiple papers and conference proceedings.

Contents

Introduction and Purpose	6
Organization and Flow	7
Terms Used In This Paper.....	7
Design Methodology Overview	8
Pre-Layout Board and Test Structure Design	9
Toolset Selection.....	13
System Design, Fabrication and Validation.....	15
Phase 1 – Pre-Fabrication Verification	15
Phase 2 - Fabrication	15
Phase 3 – Post Fabrication	17
Materials Properties Extraction.....	20
Direct Jitter Measurement and Separation	24
Preliminary conclusions on baseline measurements:.....	33
Cross-talk Measurements and Models	34
Conclusions.....	41
Concerning material properties	42
Concerning VNA and TDNA and Scope Measurements	42
Concerning Jitter and Cross-talk measurements.....	43
Closing	44
Appendix A: Material Parameters Identification	45
Appendix B: Oscilloscope Images.....	54
Appendix C: References	57

Introduction and Purpose

The design of reliable interconnects for applications above 10 Gb/s has become a complex engineering process that involves multiple interrelated steps to ensure the compliant signal integrity of the final product. By establishing high levels of confidence in the design flow by maintaining consistency throughout pre and post layout phases of development less design spins result, designs are more scalable, and future designs are created more rapidly.

The purpose of this paper is to illustrate key engineering aspects related to maintaining high level correspondence between system simulation and post layout measurements, focusing on jitter analysis correspondence with system simulation. We will address this by discussing the design of a cohesive measurement platform which consists of serial link structures which mimic both atypical and typical backplane-like pathologies. Atypical structures are not found in backplane signal paths, but are used for calibration, 3D EM model correspondence, material identification, etc. Several novel crosstalk experimental structures have been developed as well. Utilizing this hardware, and a carefully selected toolset and developed methodology, we intend to show how those steps and technologies fit together as a whole “end-to-end” process.

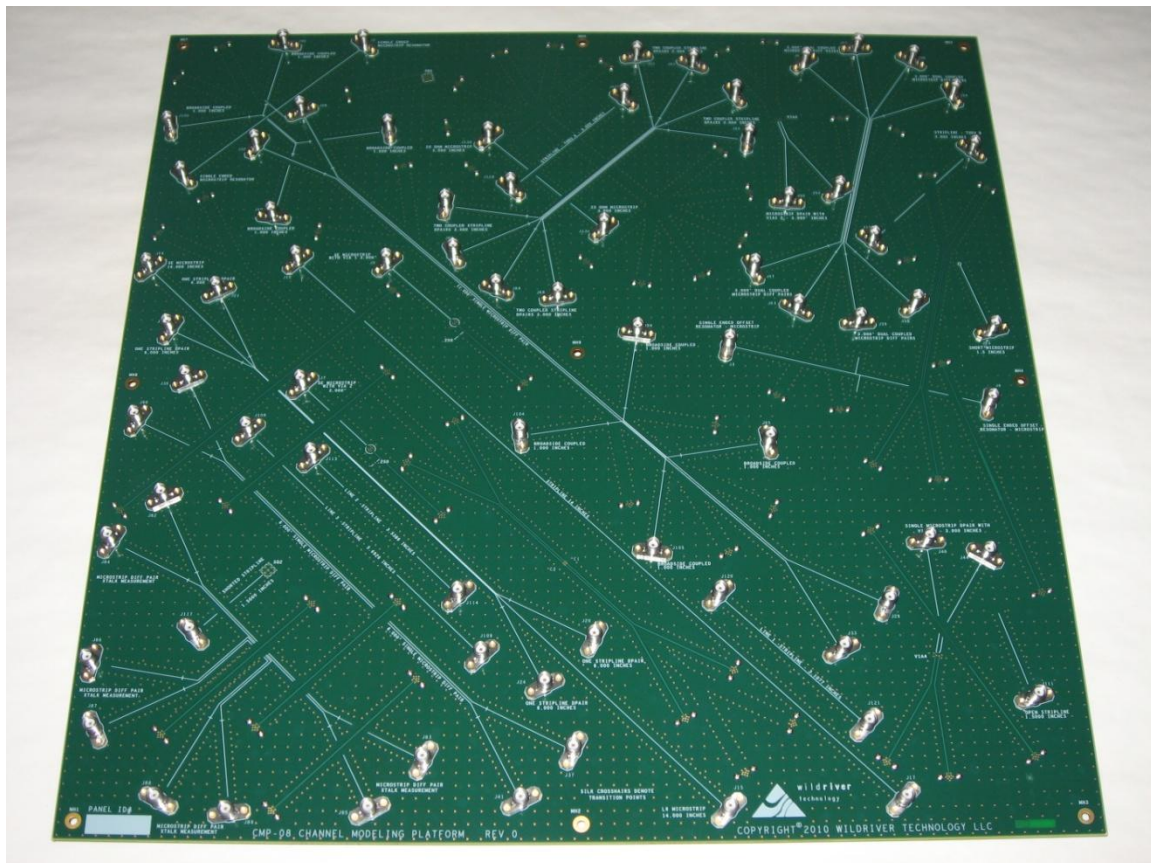


Figure 1 - The Modeling Platform as designed.

Organization and Flow

1. *Design Methodology Overview*
2. *Pre-layout board and structure design*
3. *Establish Toolset requirements*
4. *Benchmark Convolution generated eye diagrams of system simulation with that of jitter measurement equipment*
5. *Compare pre-layout simulation results with frequency domain measurements for fabricated platform*
6. *Identify material properties and establish loss models*
7. *Show improved post-layout correspondence with extracted material properties and 3D EM extracted S-parameter models*
8. *Show direct jitter measurement correspondence, including RJ-DJ extraction, to system simulation results*
9. *Conclusion.*

Terms Used In This Paper

LRM – **L**ine **R**eflect **M**atch.

SOLT - **S**hort, **O**pen, **L**oad, and **T**hru. Traditional full two calibration which typically utilizes three impedance and one transmission standards to define the calibrated reference plane.

TRL – **T**hru, **R**eflect, and **L**ine. A two port calibration which utilizes a minimum of three standards to define the calibrated reference plane. Provides the same information as a SOLT calibration via a different algorithm.

Pre-Layout Board and Test Structure Design

A test platform was conceived and a number of test structures proposed. After stackup considerations are established and reviewed with our fabrication vendor of choice the engineer typically gets some form of graphic stackup or equivalent information with associated material properties to achieve impedance objectives and manufacturability criteria (see Figure 3 - A board design starts with vendor supplied stackup and material values. below). This is required information not only to begin the design (width, separation of traces) but also to perform pre-layout estimate of all desired jitter pathologies.

We found through experimentation that these vendor produce stack-ups are at best rough estimates, but still define where you are at the pre-layout stage. The assumption early on was that we would have minimal information; no experience with prior fabricated products from the vendor selected, and that later we would compare simulations of S-parameters and system level jitter results with that of the post-layout collateral¹. This information, combined with all detail of the physical 3D configuration of the complete circuit, would then be used to understand and predict the performance of the transmission media.

Layer	Stack up	Supplier Description	Description	Stock Number	Base Thickness	Finish Thickness	er	Impedance ID	N1
1	[Copper Foil]	PSR-4000BN (semi gloss)	PSR-4000BN (semi gloss)				4.500		
		1/2 oz copper foil	1/2 oz copper foil		0.600	1.600		1, 2, 3	
2	[FR406 2116 pre-preg]	FR406 2116 pre-preg	FR406 2116 pre-preg		4.830	4.733	3.790		
		FR406 2116 pre-preg	FR406 2116 pre-preg		4.830	4.733	3.790		
3	[FR406 .014 1/1 core]	FR406 .014 1/1 core	FR406 .014 1/1 core		14.000	14.000	4.140		
		FR406 .014 1/1 core	FR406 .014 1/1 core		1.200	1.200		4, 5	
4	[FR406 2116 pre-preg]	FR406 2116 pre-preg	FR406 2116 pre-preg		4.830	3.864	3.790		
		FR406 2116 pre-preg	FR406 2116 pre-preg		4.830	3.864	3.790		
5	[FR406 .014 1/1 core]	FR406 .014 1/1 core	FR406 .014 1/1 core		14.000	14.000	4.140		
		FR406 .014 1/1 core	FR406 .014 1/1 core		1.200	1.200		6, 7	
6	[Copper Foil]	FR406 2116 pre-preg	FR406 2116 pre-preg		4.830	4.733	3.790		
		1/2 oz copper foil	1/2 oz copper foil		0.600	1.600		8, 9, 10	
		PSR-4000BN (semi gloss)	PSR-4000BN (semi gloss)				4.500		
Copper Thickness = 8.000 Dielectric Thickness = 54.662 Overall Processed Thickness = 62.662									

Impedance ID	Structure Name	Impedance Signal Layer	Ref. Plane 1 in Layer	Ref. Plane 2 in Layer	Lower Trace Width	Upper Trace Width	Trace Separation	Lower Ground Strip Width	Upper Ground Strip Width	Ground Strip Separation	Calculated Impedance	Target Impedance	Tol (+/- %)
--------------	----------------	------------------------	-----------------------	-----------------------	-------------------	-------------------	------------------	--------------------------	--------------------------	-------------------------	----------------------	------------------	-------------

Figure 3 - A board design starts with vendor supplied stackup and material values.

Once stackup layers were defined impedance objectives were established. First generation fabrications have only materials, stack up, and estimated material properties established. The assumptions concerning the material properties had now been made by the engineers. The team arbitrarily decided on a target value of 5% minimum cross-talk from aggressor to quiet victim. All parties reviewed this proposal and the project was moved forward to the layout process. Figure 4 shows what the fabrication vendor provided in terms of materials estimates and stackup for their process:

¹ Post-layout collateral consists of hardware, extracted material properties, and loss models for all structures.

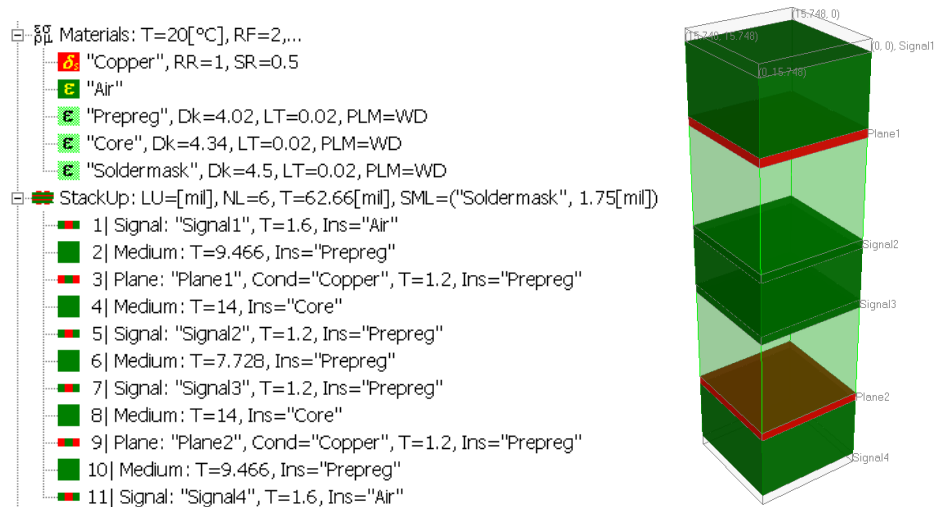


Figure 4 Fabrication vendor’s CMP-08 board materials and stackup in Simbeor 2011

Some structures were intended to permit simple benchmarking experiments for material extraction. Others were designed to produce more detailed and complex crosstalk scenarios. A summary of the relevant test structures and their function is described in Table 1 below.

Structure	Intended Purpose
Singled Ended Microstrip and Stripline Trace Structures, 3 to 14 inch lengths	Used for extraction of material properties (Dk and LT) using Simbeor 2011.
Differential Microstrip and Stripline Trace Structures, 3 to 11 inch lengths	Used for loss model verification in both Pre and Post layout (post layout uses extracted material properties). Also used for relating simple ISI (“deterministic jitter”) for comparison, measurement versus system simulation.
Neves Pathological	Simple imbalanced 3 inch DIFF transmission with crosstalk aggressor. Used to analyze impact of impedance degradation due to coupled trace, mode conversion and added crosstalk aggressor.
McMorrow Coupler	Emulates the equivalent of several strong aggressors in three places along a differential stripline interconnect. Used to evaluate real interconnect cases with the inclusion ISI (“deterministic jitter”) for comparison, measurement versus system simulation.

Table 1 –Summary of channel modeling platform test structures relevant to this paper

Single Ended Trace Structures

Single ended transmission lines are basic elements used for material extraction and also serve as impedance test coupons for making 50 Ohm airline calibrated measurements of

board impedances. They are also used for localizing the reference plane very close to test structures using TRL/LRM calibration methodology, although this capability exists. The resulting pre and post layout S-parameter model, either 3D EM extracted or lab measured, included all launch and T-line impact. Accordingly, for the purpose of this paper only SOLT calibration was performed.

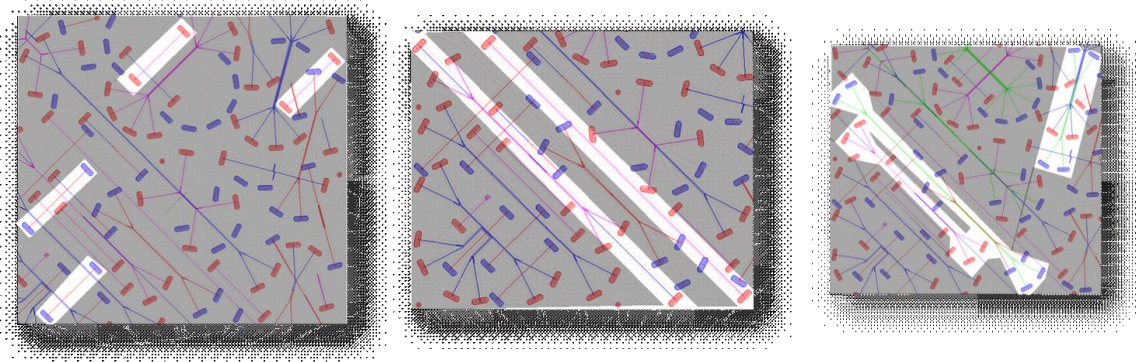


Figure 5 - (left) 14 inch Single-ended Test Structures, Microstrip and Stripline, (center) 14 inch Single-ended Test Structures, Microstrip and Stripline, and (right) Differential Stripline Trace Structures, Single Pair, 3, 6, and 11 inch lengths

Differential Trace Structures

There are numerous differential structures of both microstrip and stripline configuration, ranging from 3 inches to 11 inches in length, where each SMA transition into the structures is 1.5 inches long. The differential topology provides the ability to compare against the differential via field, and confirm loss modeling.

Special Coupling Structures

There are two significant structures aimed at more complex crosstalk cases (see Figure 6 - Layout of Neves Pathological Test Structure (left), and McMorrow Coupler (right)), one designed by Al Neves, and the other by Scott McMorrow.

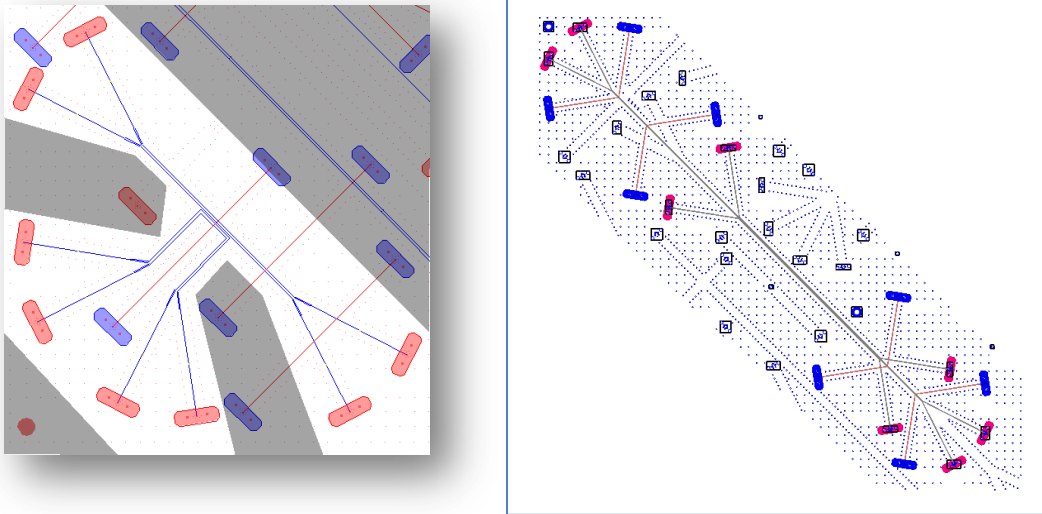


Figure 6 - Layout of Neves Pathological Test Structure (left), and McMorrow Coupler (right)

Neves Pathological Coupling Structure

Crosstalk is commonly thought of in terms of aggressor energy coupled conceptually through capacitive and inductive mechanisms, but aggressor traces also alter impedance, symmetry, and create modal conversion from differential to common mode. The Neves Pathological crosstalk structure serves to explore this nature of crosstalk.

The Pathological crosstalk structure consists of 3 inches of microstrip differential victim trace, just like the microstrip differential THRU, but with the addition of a 1 inch coupled microstrip aggressor pair. By simply adding this one aggressor jitter, S-parameters, and modal conversion can easily be analyzed by 3D EM or measurement, for a simple yet pathological structure. This structure creates symmetry imbalance, resulting in increase jitter even with no crosstalk aggressor energy.

McMorrow Coupling Structure

Typical backplane and midplane based interconnect channels include multiple line cards attached to an interconnect board through electrically large connectors. Crosstalk isolation in high speed connectors has improved in recent years, but there are always opportunities for neighboring aggressive nets to induce crosstalk into a victim through coupled routing within the connector breakout region, within the connector, and within the via breakout fields. These sections are often relatively short, with lengths less than 1 inch, but can often have high coupling coefficients. Within each connector field there can be as many as 8 nearest neighbor aggressors, comprising the 8 differential signals surrounding a connector in the adjacent rows and columns. In addition, there may be two same layer aggressors on the midplane on either side of a victim trace.

It is generally not feasible to instrument 8 aggressors on each end of midplane, along with two aggressors on either side of a victim, in a small compact structure that is both easy to

measure and to model. However, it is possible to emulate the equivalent of several strong aggressors in three places along the interconnect: at the equivalent of the Tx side connector, at the Rx side connector equivalent, and in the backplane trace routing section between the two connectors. The McMorrow Coupler was designed for this purpose; simplified evaluation of real interconnect cases with the inclusion of complex crosstalk induced DDJ.

In the McMorrow coupler, an 11 inch long differential stripline is coupled into a one inch long broadside differential pair with a high coupling coefficient of $> 20\%$, a value of coupling high enough to induce the equivalent crosstalk typical for worst case correlated aggressors. Tx aggressor drivers can be placed preferentially on the near end side of the coupler to simulate Tx-to-Tx same direction crosstalk, or on the far end side to simulate Tx-to-Tx opposite direction crosstalk. This second type of crosstalk can create significant far end crosstalk at the receiver. A duplicate broadside coupler is also placed at the far end receiver side of the 11 inch long victim, to simulate additional crosstalk on the receiver side. Again, aggressor Tx port placement can be used to simulate Tx transitioning in the same direction as the Rx received waveform, which is the most favorable configuration, or in the opposite direction, which causes maximum received crosstalk.

Offset from the center of the victim pair is a 5 inch long coupled differential aggressor on the same stripline layer, split to surround the victim on each side. This side-to-side split provides a 2X amplification of the injected differential mode crosstalk, as seen by the victim. The center coupled section is designed to have asymmetric placement, directly adjacent to the broadside coupler on one side of the interconnect, and about 3 inches away from the coupler on the other side. Because no effort was made to adjust victim characteristic impedance in the coupled section, the offset placement of each coupled section presents a complex impedance reflection profile to the interconnect, along with complex superposition of the crosstalk waveforms injected into the victim channel. These channel complexities are, however, designed to be easily modeled with commercial full wave electromagnetic solvers, and measured with conventional time and frequency domain instruments.

Toolset Selection

The following provides the reasoning behind why we used certain tools. In some cases tools were used simply because of availability, but in other cases we had specific criteria in mind based on the project's goals. Our project goals were clear and unambiguous; consistent simulation methodology related to direct measurements, which include jitter analysis of low probability crosstalk, RJ-DJ, eye diagram overall fidelity, S-parameters, and TDNA or time domain to 10Gbpsec at both pre and post layout stages. For 10Gbpsec data rates we decided a minimum requirement of simulation measurement corresponds to a factor of 5 from Nyquist Frequency of 5GHz for a 10Gbpsec NRZ base-band data stream., so we were essentially shooting for 25GHz and a consistent measurement and simulation methodology.

Our Requirements:

- **3D EM analysis:**
 - Ability to extract S-parameter models for 3D structures
 - Causal and accurate loss modeling – multi-pole or wideband Debye
 - Broadband conductor loss and dispersion models
 - Conductor surface roughness modeling. (Important but not as vital if we plan on using low loss dielectrics)
 - General 3D EM analysis that passes some extensive benchmarking of simple test structures loss
 - Ability to identify material properties with some concerted methodology
 - The ability to compare measure data that is test for passivity/causality (Very important for insuring measurement integrity)

Simbeor2011 was utilized along with CST for 3D EM launch extraction

- **System Simulation Toolset:**
 - Convolutional simulator for simulating stimulus and S-parameter model of channel
 - Generate meaningful eye diagram simulations
 - Eye diagram jitter and fidelity consistent with scope eye diagram simulation convolution simulator

Synopsis HSPICE was utilized for system simulation.

- **VNA, Vector Network Analyzer**
 - SOLT calibration effective past 25GHz, preferable 40GHz
 - 4 port S-parameter capability
 - 12-port capability would have made crosstalk analysis of differential structures more convenient
- **Time Domain TDNA (LeCroy SPARQ 4004E)**
 - Equivalent frequency domain bandwidth of 40GHz
 - Assist with topologically identify impedance discontinuities in test structures, evaluation of launch discontinuities
 - Easy measurement of impedance profile, both single-ended and differential
 - 4-port passive/causal S-parameter measurements
 - S-parameters correctly correspond to test platform Beatty standards
 - 6psec risetime, 40GHz bandwidth
- **Digitizing Oscilloscope: (LeCroy SDA 830 zi)**
 - Real-time, 80 GS/s recording
 - Dual input 30GHz analog bandwidth
 - Quad input 16GHz analog bandwidth

- “channel” and “fixture” emulation and de-embedding software
- Jitter measurements
- **10Gb/s Data Pattern Generator (Centellax TG2P1A)**
 - One diff pair, <25ps rise-time output pair
 - Clock-out and Clock in for synchronizing multiple pairs
 - Multiple PRBS data patterns

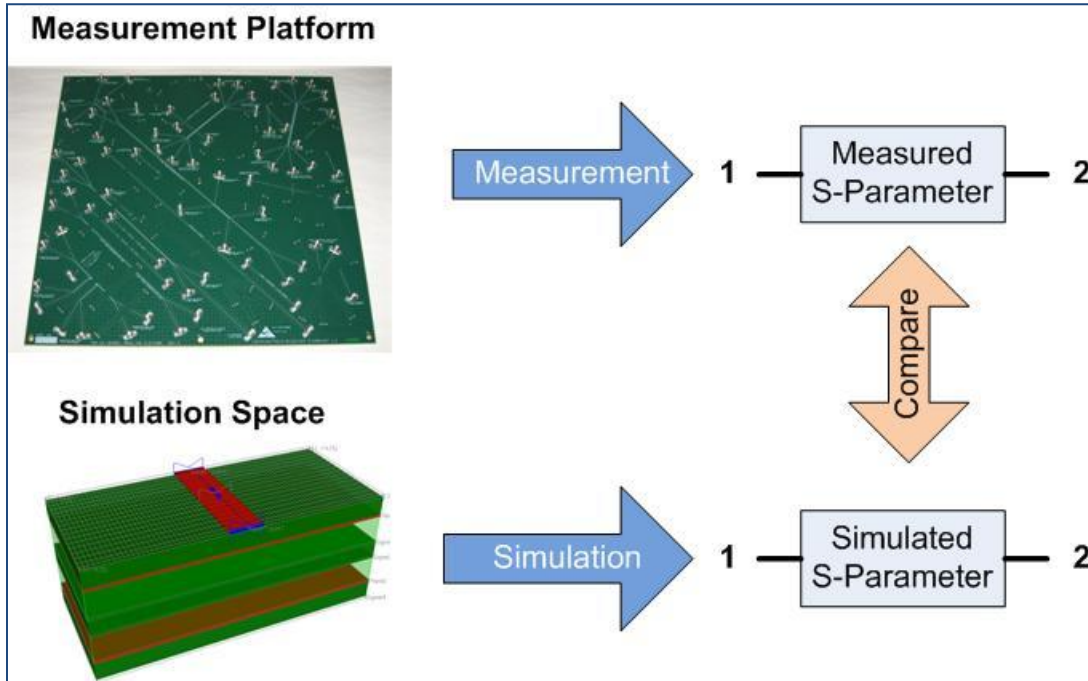


Figure 7 – Measurement versus Simulation Space correspondence requires: first benchmarking with simple structures, good material properties, good VNA or TDNA calibration, and good loss models

System Design, Fabrication and Validation

Phase 1 – Pre-Fabrication Verification

Before moving on to fabrication, some preliminary test structure S-parameters were analyzed to ensure our coupled structures would provide the substantial cross-talk component we desire in the final board. Estimations were also made via 3D “field solvers” of the scattering parameters for the structures going on the CMP-08 platform, prior to fabrication. This procedure required physical material properties D_k and LT of all materials (pre-preg, core, solder mask), as well as a layout of the measurement platform.

Phase 2 - Fabrication

Of course the actual production of the test platform required many weeks, but during that time there was much we could do to prepare for the actual hardware.

Using the S-parameter data produced by two different field solving packages, we were able to predict the probable performance of each of our test structures with regard to signal integrity, including jitter² and crosstalk. To do this within the oscilloscope we employed a behavioral simulator to confirm our jitter extraction algorithms³. We used this simulator and its “embedding/de-embedding” technique to simulate the behavior of a single data channel and multiple data channels through the “virtual” circuit. Using simulated signals are used as a stimulus, the s-parameters were emulated in the signal paths, and eye diagrams were then constructed and jitter measurements were taken. Since this kind of simulation is not limited by practical considerations (like having a limited number of aggressor channels) nearly infinite flexibility in the victim and aggressor signal characteristics was possible and therefore many experiments for simulation of crosstalk would be possible.

During this phase of our work we were able to compare “noiseless” eye diagrams using both oscilloscope software as well as SPICE simulations using the same assumptions concerning the stimulus signal shape. For our purposes, at this time we assumed a 25ps 20-80% rise time and a 10Gb/s serial data stream.

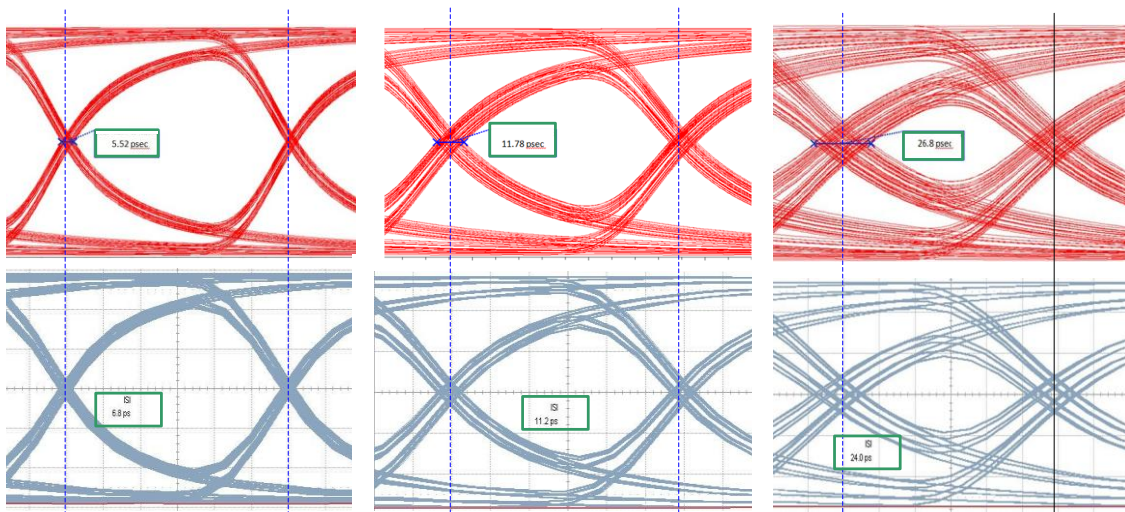


Figure 8 - Differential stripline (left) 3 inch, (center) 6 inch and (right) 11 inch. The red “noiseless” eye diagrams are from SPICE, the blue are from simulation and channel emulation in an oscilloscope.

Using the pre-fabrication Simbeor scattering parameters, Jim and Marty did many simulations independently to confirm the modeling and simulation tools were in agreement. At first we were not able to obtain a close correspondence between the spice and oscilloscope eye diagrams and Inter Symbol Interference (ISI) components of the

² In most cases, where jitter of a passive circuit board is concerned, we can only infer the deterministic part of jitter which is induced by losses entirely described by the scattering parameters for the structures or networks under study.

³ Martin Miller is the author of the behavioral simulator used for this purpose.

deterministic jitter. The shapes were right but the ISI numbers were not close enough for comfort. However once we also agreed that these simulations must be performed using identical test patterns (we settled on the pseudo-Random Bit Sequence PRBS7) the deterministic jitter numbers and shapes of the eye diagrams were found to be quite compatible. Essentially this is because the longest run-lengths (length of a sequence of identical bit states), and changes between short run-lengths and long-run lengths dominate the ISI measurement⁴.

The eye diagrams shown in Figure 8 - Differential stripline (left) 3 inch, (center) 6 inch and (right) 11 inch. The red “noiseless” eye diagrams are from SPICE, the blue are from simulation and channel emulation in an oscilloscope. above show only graphical results for PRBS7, but to drive home the point about how ISI (a component of deterministic jitter) varies with the test pattern used, we produce here tables of results from the same simulations for various test patterns and also for the Microstrip structures, which are mostly overlooked for the rest of this paper.

	Structure	3" MS diff	6" MS diff	11" MS diff	3" SL diff	6" SL diff	11" SL diff
	Parametric	ISI (ps)	ISI (ps)	ISI (ps)	ISI (ps)	ISI (ps)	ISI (ps)
LeCroy Simulator	PRBS7	2.90	6.10	13.60	5.60	10.20	25.00
HSPICE	PRBS7	3.29	6.01	13.64	5.52	11.78	26.80

Table 2- ISI estimations from pre-fabrication models for the 6 varieties of differential structures.

Structure	3" MS diff	6" MS diff	11" MS diff	3" SL diff	6" SL diff	11" SL diff
Parametric	ISI (ps)	ISI (ps)	ISI (ps)	ISI (ps)	ISI (ps)	ISI (ps)
PRBS5	2.80	6.00	13.30	5.40	10.00	24.50
PRBS7	2.90	6.10	13.60	5.60	10.20	25.00
PRBS9	3.20	6.20	14.00	5.80	10.90	26.10
PRBS15	3.40	6.60	14.20	5.70	10.90	25.70
PRBS31	3.40	6.80	14.10	5.90	10.90	25.80

Table 3- LeCroy Simulator ISI predictions from pre-fabrication models

Phase 3 – Post Fabrication

Once the fabrication of the board was complete we proceeded to confirm the predictions and determine to what degree of confidence we could properly ascribed to those predictions. There were two goals to this part of the research:

1. Confirm that measured S-parameter sets confirm the assumptions about material properties, and if not resolve these discrepancies (see “Materials Properties Extractions”)
2. Confirm that the signal integrity measurements correspond to the pre-fabrication predictions, and if not resolve these discrepancies.

⁴ This is an often overlooked fact: The ISI component of deterministic jitter depends strongly on the test pattern with which the network is tested. Essentially this is because the longest run-lengths (length of a sequence of identical bit states), and changes between short run-lengths and long-run lengths dominate the ISI measurement.

This first part consists of direct measurement of the scattering parameters for test structures both TDR and VNA instruments. Some measurements were performed using a 4-port 40GHz TDNA (LeCroy SPARQ) while the VNA measurements were made with a 4-port 40GHz Anritsu Instrument. By necessity we had to use two different CP-08 boards but they were from the same prototype run, with connectors from the same manufacturer's batch, and the connectors were installed onto the board in the same facility.

It turns out the agreement of these measurements was quite good. See Figure 9, Figure 10, and Figure 11 below.

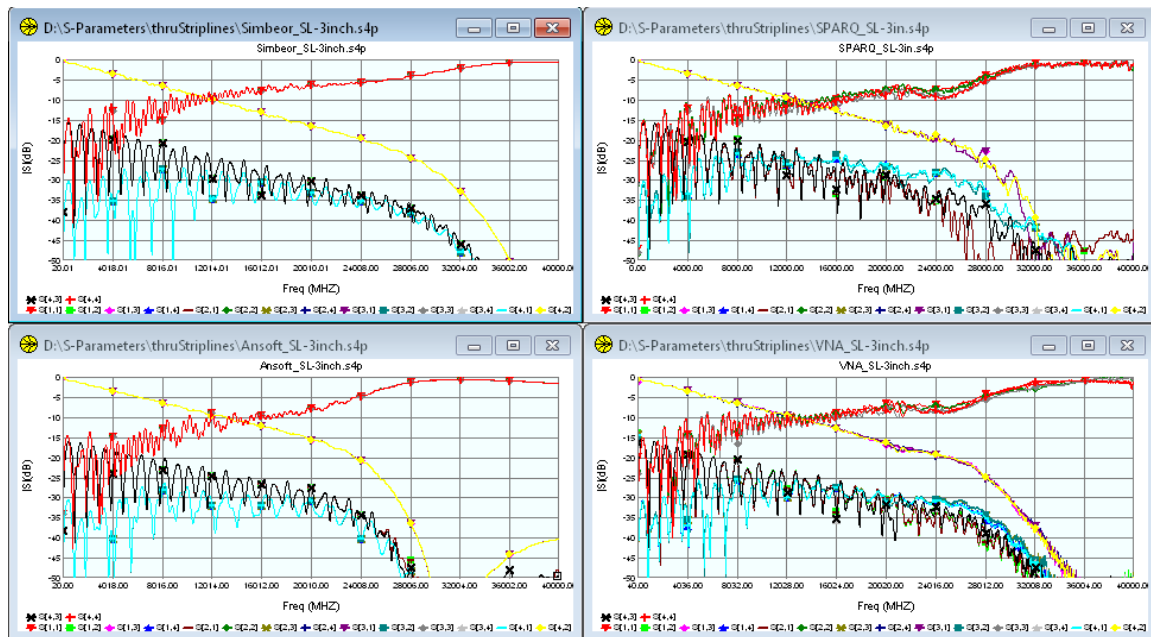


Figure 9 - Results of S-parameter comparisons from models and from VNA and TDNA for the 3 inch differential stripline.

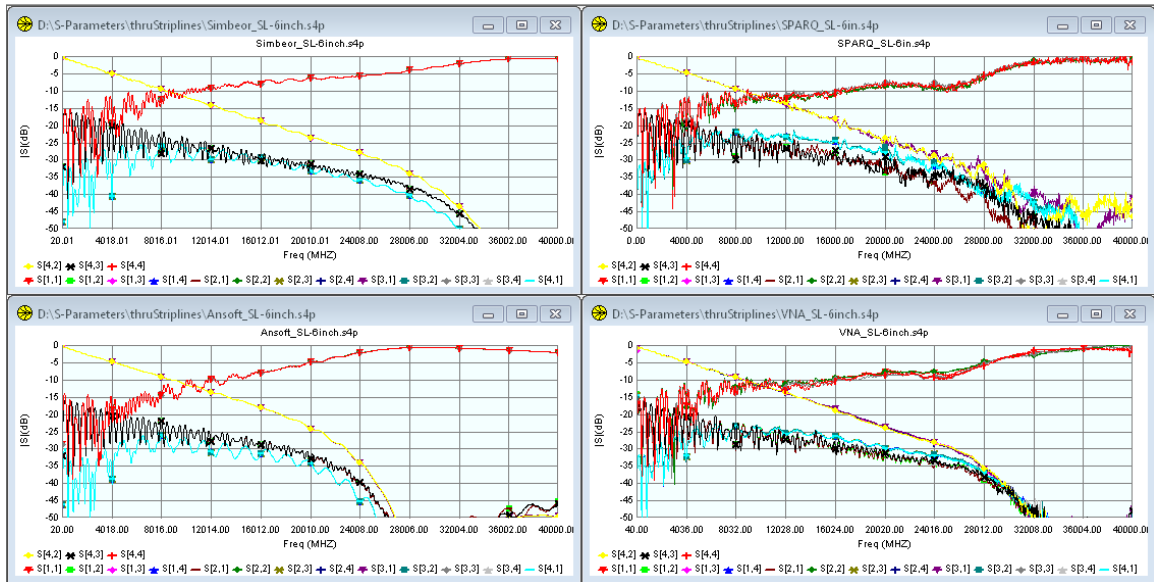


Figure 10 - Results of S-parameter comparisons from models and from VNA and TDNA for the 6 inch differential stripline.

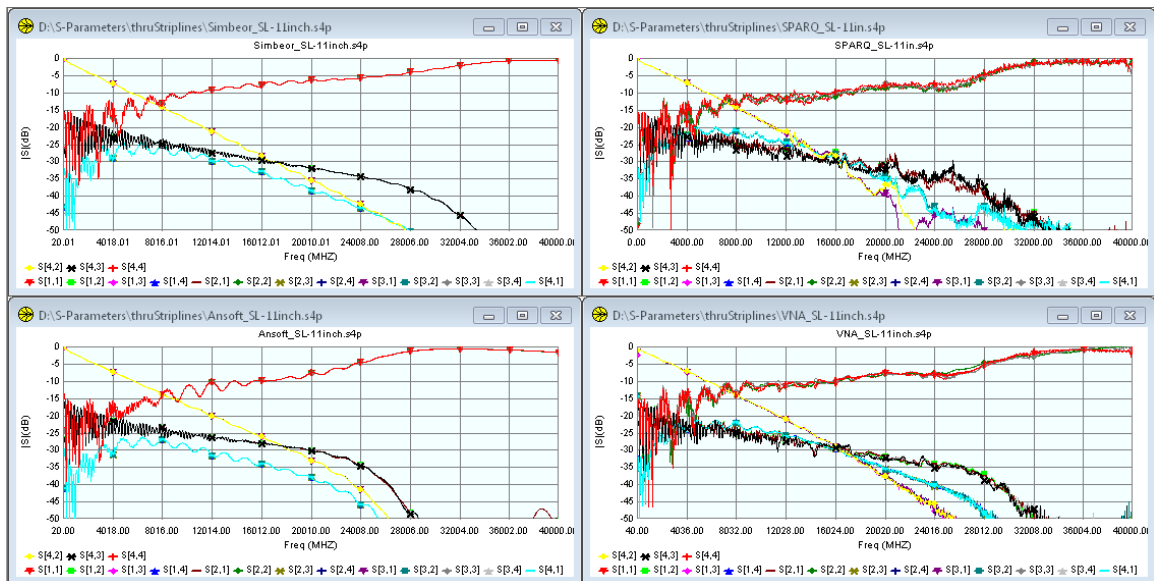


Figure 11 - Results of S-parameter comparisons from models and from VNA and TDNA for the 11 inch differential stripline.

The differences in these are explained in the materials extraction and identification process described below. Initial and identified dielectric parameters can be found in Table A.1 in the Appendix A.

Materials Properties Extraction

Here is one of the very interesting subjects about which some of the authors have written about previously [1], [2]. Manufacturers of low-cost PCBs typically provide a value of dielectric constant typically at one frequency.

Since the goal of this project is to define high-confidence design methodology for meaningful jitter extraction, we needed a concerted methodology for obtaining Dk and LT over a 25GHz bandwidth.

The older method discussed in 2009, [1, and 2] involves:

- Line segments or low reflective structures (very low $S[1,1]$)
- Resonant structures or high reflective structures with clear resonances in $S[1,1]$
- To identify dielectric properties we first measure and utilize TRL/LRM calibration to remove launch and loss impact, moving the reference plane very close to the specific structure
- Perform iterative 3D EM simulations while changing Dk and LT to converge on both return and insertion loss

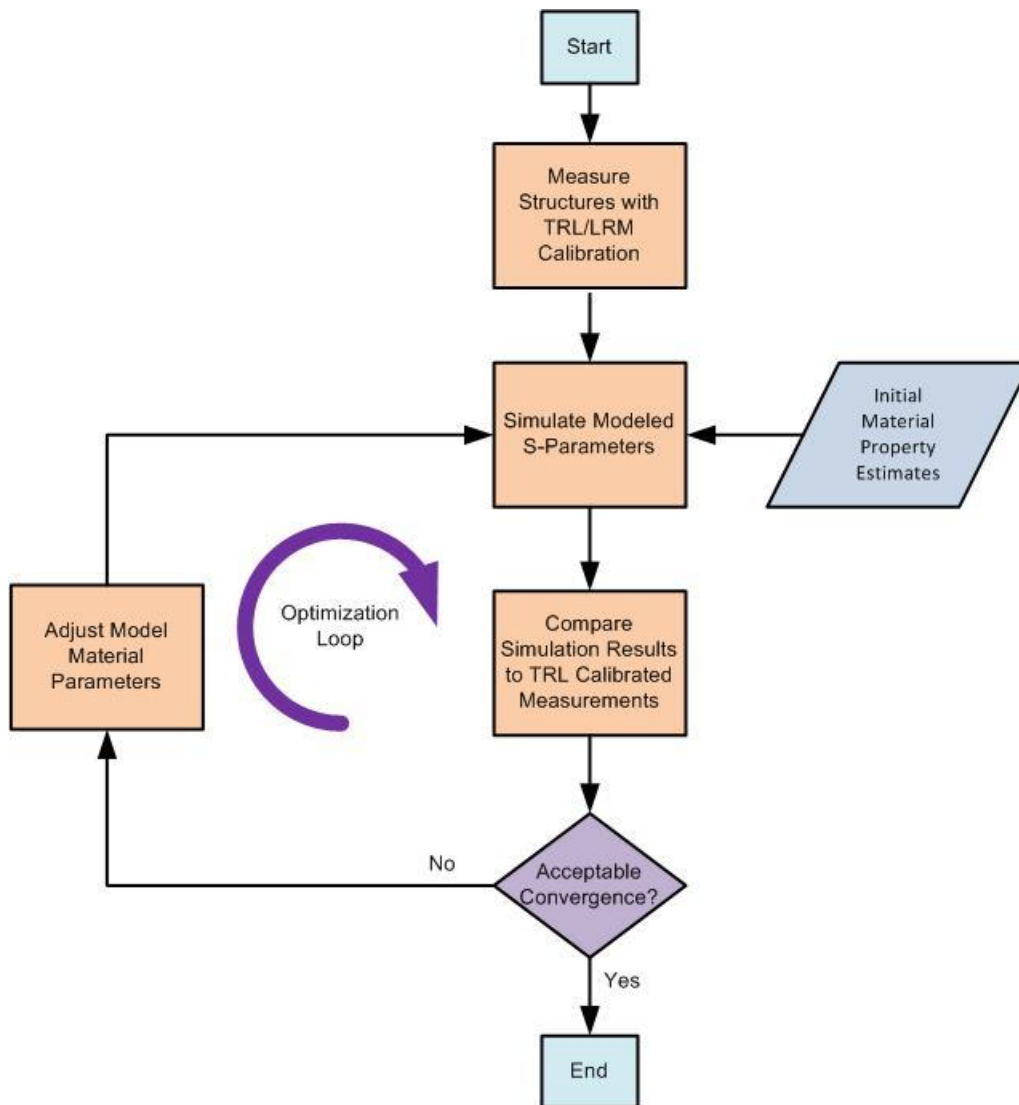


Figure 12 –The old process flow for optimizing the material parameters for a given measured S-Parameter

The older method relied on a methodology as outlined in Figure 12 which relied on TRL calibration, whereas the new method requires only simple SOLT calibration. TRL/LRM makes the older method cumbersome, error prone, and requires numerous on board calibration structures (LINE1, 2,3 THRU, OPEN, LOAD).

The new material identification method (see Figure 13) is based on comparison of the GMS-parameters extracted from the measured data with GMS-parameters computed for a line segment without launches or connectors. Additionally, there is no requirement to know the impedance of the t-line, which is required when using the former TRL/LRM method. The key in such comparison is the minimal number of the parameters to match. Only generalized modal transmission parameters are not zero and are used for identification. Both computed and measured generalized reflection and modal transition

parameters are equal to zero exactly. It simplifies the identification process a lot without sacrificing the accuracy and make the GMS-parameters method the simplest possible.

PCB dielectrics are inhomogeneous, usually a mixture of glass and epoxy that can be characterized either as the mixture of two models or, more often, with an effective dielectric model. The reasons are numerous:

1. Space between traces in coupled microstrip lines may be filled with the solder mask dielectric material with properties different from the substrate dielectric material.
2. Prepreg and core layers in stripline configurations may have different dielectric properties. Space between traces in coupled striplines may be filled with either epoxy or air depending on the manufacturing technology.

For these reasons, use of one effective dielectric model may not be accurate enough for analysis of coupled lines and for the cross-talk analysis. For accurate characterization of coupling effect you may need to identify and use parameters of at least 2 dielectrics (or, more preferable, a more accurate model) or you may need to use one anisotropic dielectric model in case of striplines.

We used GMS parameters of coupled lines for identification of material properties suitable for accurate simulation of multi-gigabit signals in differential and coupled interconnects up to 20-25 GHz. Our updated dielectric model properties were then used to validate analysis with the measurements for different coupled differential structures. Fundamentally, this stage of the process modifies the assumptions made during the first phase of the process concerning the properties of the materials, and even the geometry assumptions of the second stage.

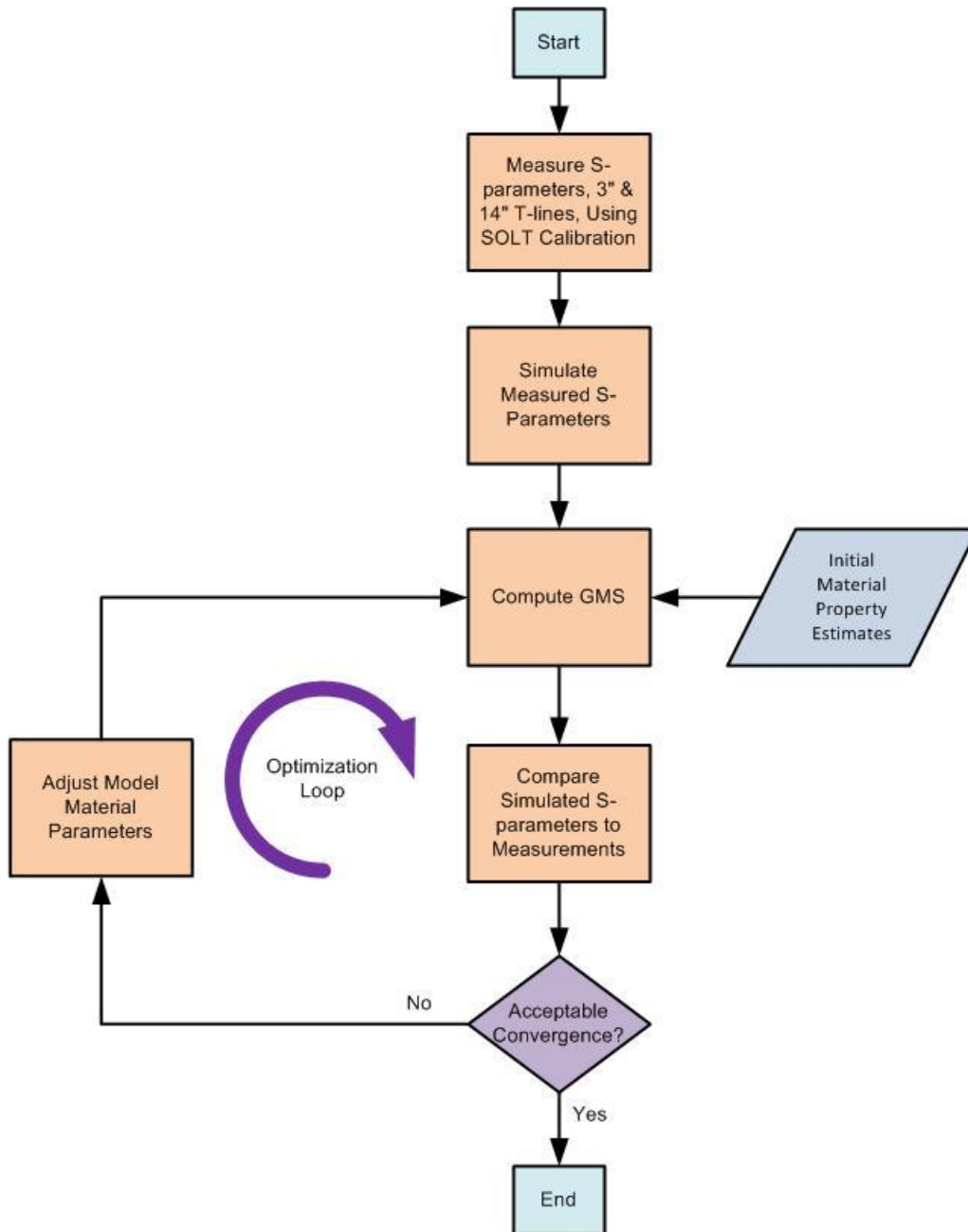


Figure 13 – New GMS method of material extraction.

In broad strokes, comparison of specific features of the predicted versus the observed S-parameters, the assumptions concerning the DC-resistance (cross-section and conductor resistivity) were adapted. The dielectric constants of insulator layers were then adapted to match impedance differences and group-delay.

Direct Jitter Measurement and Separation

The jitter extraction tools and algorithms (largely written by M. Miller) are those from a LeCroy Oscilloscope. While several variations of the algorithms for Random Jitter (Rj) are available, the only one used here is the “industry standard” spectral method. This allows for direct comparison and compatibility with other oscilloscope vendors. It is the experience of this author that this method yields reasonable results under most circumstances even though it has some weaknesses [8].

Summary for the overall procedure:

1. Digitized waveform data is digitally processed to “de-embed” cables and fixtures, which are to be excluded from the measurement.
2. The differential signals (in all cases here) are processed for threshold crossing times, and a “virtual receiver” performs Clock Data Recovery (CDR) for the purposes of synchronizing the eye-diagrams and jitter histograms.
3. Pattern detection is performed on the observed sequence (when a repeating pattern is present) of edges. Time Interval Error (TIE) sequence is thus correlated with a specific sequence. The systematic TIE values is learned, and then removed from the sequence of edge times to provide a time error sequence representing both random jitter and “bounded uncorrelated” jitter, $R_j + BU_j$. The systematic variations in TIE are analyzed to produce both the Inter Symbol Interference (ISI) and the Data Dependent Jitter (DDj) parameters (defined in greater detail below)
4. This resulting function of time is spectrally analyzed, and two assumptions are made.
 - a. All identified “peaks” in the spectrum are “deterministic”
 - b. The remaining “background” represents purely random jitter.

For these measurements a 30 GHz real-time oscilloscope was chosen. For reasonable fidelity in the shapes for the eye-diagrams it is an industry “rule of thumb” to have at least the fifth harmonic of the frequency for a 10101010... pattern. For the 10 Gb/s studies we are doing, this requires at least a 25GHz analog bandwidth.

The Centellax ~10Gb/s generator (TG2P1A) was used for both the baseline measurements and for the crosstalk measurements. Two such generators can be phase-locked easily, which is critical to the most interesting cases of neighbor to neighbor crosstalk.

It is important to mention the care that needs to be taken in handling high-quality cables, terminations, splitters and instrument inputs. We will not teach those details in this paper, but suffice it to say you must take care in assembling cables and making connections to not damage them and to obtain repeatable results. Standard practices must be followed with attention to detail. During the work for this paper one SMA feed-thru was found to be damaged and falsified the first round of characterizations for the cables connecting the test board to the oscilloscope. Every termination was tested and every cable to assure accurate de-embedding.

First we examine some baseline measurements, to see if observations correspond to expectations. The generator was used with some high quality cables to stimulate the 3” differential stripline mentioned above with a 10Gb/s data stream with PRBS7 (as we used in simulations) . Four measured 2-port (s2p) files for the connection cables and the modeled s2p for the stripline connector and “launch” (provided by Scott) were combined to form a single s4p file representing the measurement “fixture”. An LeCroy-internal tool was used to perform this compilation of 5 2-port(s2p) S-parameter sets to produce a single 4-port (s4p). The fixture de-embedding feature of the oscilloscope was then used to mathematically remove the effect of the cables and launch so that we could directly compare measurement results with initial pre-fabrication predictions. This last process is called “fixture de-embedding” and is available for most high-end oscilloscopes. The diagram below shows how this was configured.

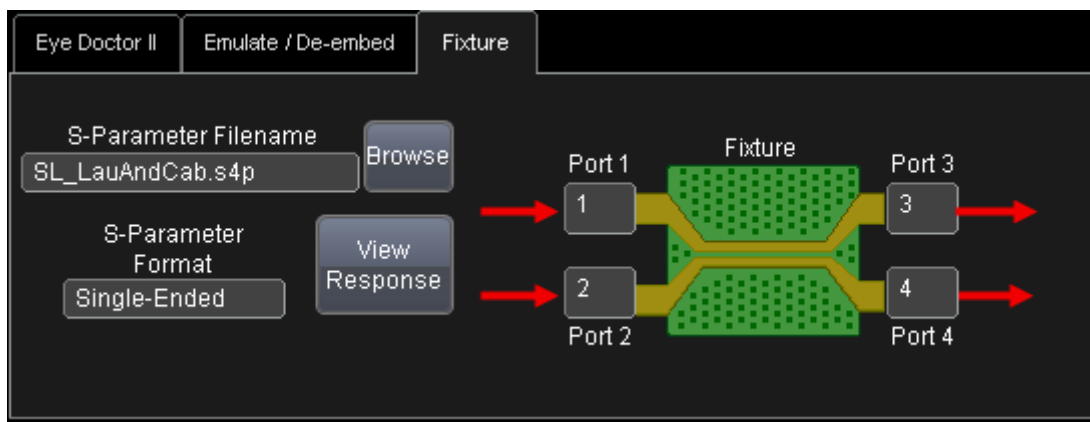


Figure 14 - De-embedding of the cables, connectors and”launch”. The effect of this extra step is worth 1 to 2 ps in the ISI measurements made.

Before comparing results, let’s be clear about the terms for the measurement we will compare. The effect of a printed circuit structure (sometimes called a “channel”), is that it has a time-domain impulse response which extends beyond a single bit-period, and in many cases extends beyond many bit periods. This effect is sometimes called “Inter Symbol Interference” or ISI. There are two common parametrics which are commonly associated with this effect. One is DDj and the other is ISI. The definitions (originally attributable to Agilent, but paraphrased) are:

- Dependent on the position within a repeating sequence of data “bits”, each edge will have a systematic displacement in time (early or late) from the ideal edge timing.
- “Data Dependent Jitter”, DDj is the difference between the earliest and the latest systematic edge-time-displacement for all edges.
- The ISI value is the larger of the difference between the earliest and the latest systematic edge-time-displacement for positive edges only, or for negative edges

only. Or, in other words the larger of the peak-peak time shifts of either positive or negative edge slopes.

It should be obvious that the ISI value is always less than or equal to DDj. When they differ significantly, it is due to some asymmetry in the signal shape or an error in the threshold use for determining the edge timing.

So, measurements were made. It was somewhat puzzling that this eye diagram and jitter measurement did not correspond to our initial pre-fabrication estimations. The ISI (data dependent jitter contribution) was expected to be closer to 5 or 6 ps, and instead is about 11 ps, and that when the cables, connectors and “launch” are de-embedded. One essential reason for this apparent difference is that our signal source (stimulus for the modeling) was “perfect” with regard to its own Data Dependent Jitter or DDj (if measured with no embedded channel whatsoever). The harsh reality is that: no real generator is free from some amount of “inherent” ISI. We can imagine a number of reasons this is true, The generator itself has some printed circuit and probably a bit of cable or at least a “launch” (from the PC board to an output connector). Moreover, the digital circuitry required for generating the digital pattern (in this case various PRBSx) introduces digital feed-back which manifests as a pattern-dependent “jitter”. Following this observation, several other generators were tested, and while one could hope larger more expensive instruments would provide better performance in this regard, they did not (no names will be named).

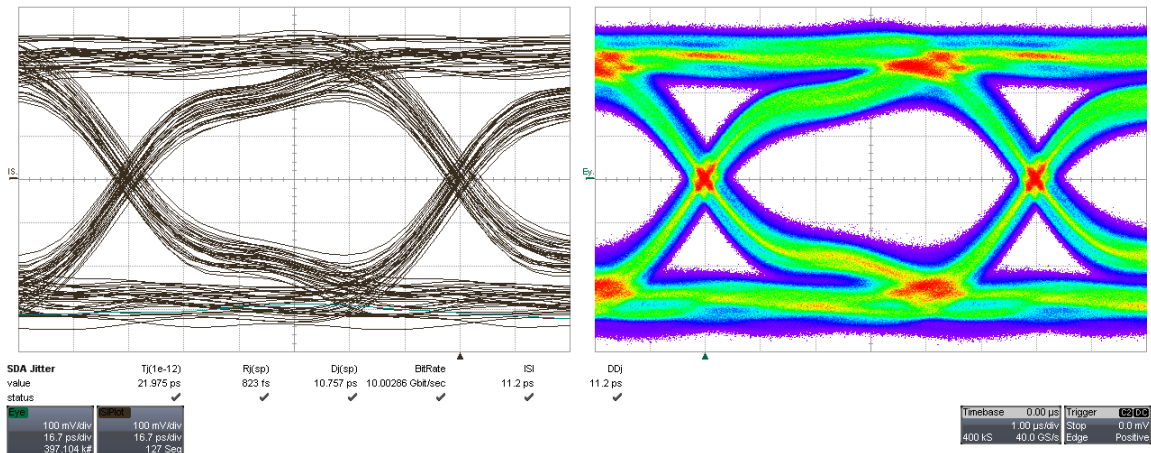


Figure 15: Direct measurement of Centellax™ (TG2P1A) Generator through 3” differential stripline with cables, connectors and launches de-embedded. The ISI measurement is 11.2ps, whereas the simple prediction using an ideal stimulus was 5.8ps. How is the apparent difference explained?

When the generator was measured directly (also good cables that were de-embedded ... making hardly much difference) it was evident that there was already a data-dependent jitter and significant structure in the noiseless eye-diagram. In other words, the signal generator was imperfect with regard to ISI and DDj before you even begin to pass the generator signals through a printed-circuit structure.

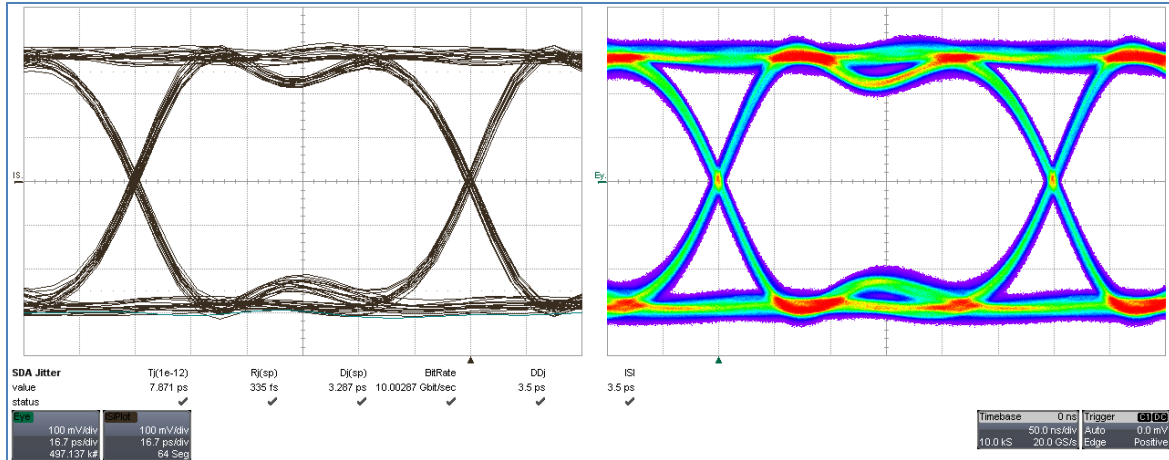


Figure 16 - Direct measurement of Centellax™ (TG2P1A) Generator with no test structure both pairs of cables used in other measurements). The ISI measurement is 3.5ps all by itself, and DDj is the same.

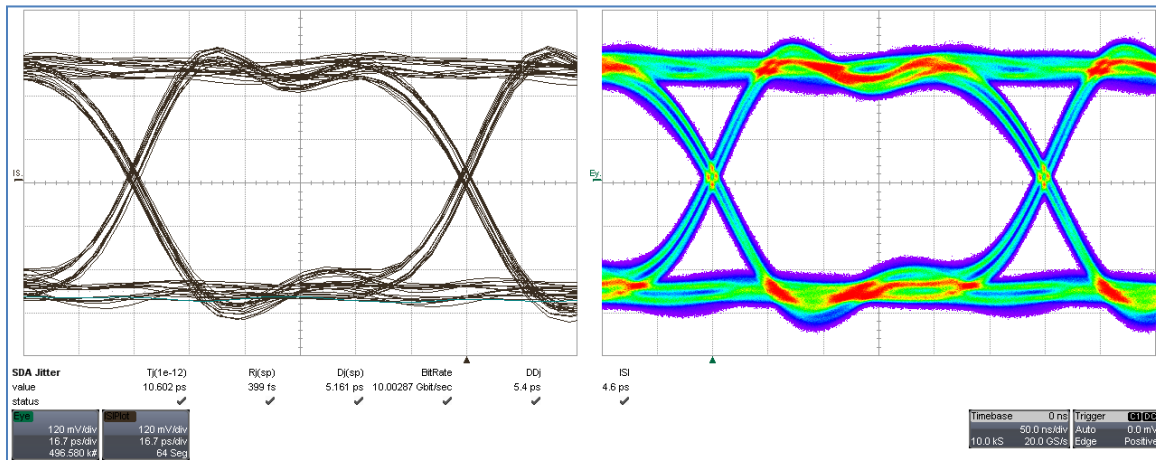


Figure 17 - Direct measurement of Centellax™ (TG2P1A) Generator with no test structure with de-embedded cables (both pairs used in other measurements). The ISI measurement is 4.6ps and DDj is 5.4ps ... a surprise since they are less without the cables de-embedded

Direct measurement of Centellax (no PC structures, just one pair of high-quality cables between the generator and the oscilloscope), shows an “inherent” ISI contribution. And we learned we were not going to obtain a better (in this regard) generator with which to perform all the measurements we required.

Lacking an ideal real signal source, the recorded signal was thereafter used as a stimulus to the Monte-Carlo simulator, rather than an “ideal” signal source, and “embedding” or “Emulating the channel for the 3” differential stripline (see figure X). The resulting measurements are called Co-simulations, because they use both real measurements and simulated channel behavior.

So these Co-simulations combine the information obtained either through 3D solvers and TDNA or VNA measured S-parameter sets, with the measurement data obtained with the real-time oscilloscope.

3 inch Differential Stripline Comparison of Noiseless Eye Diagrams, ISI and DDj jitter figures.

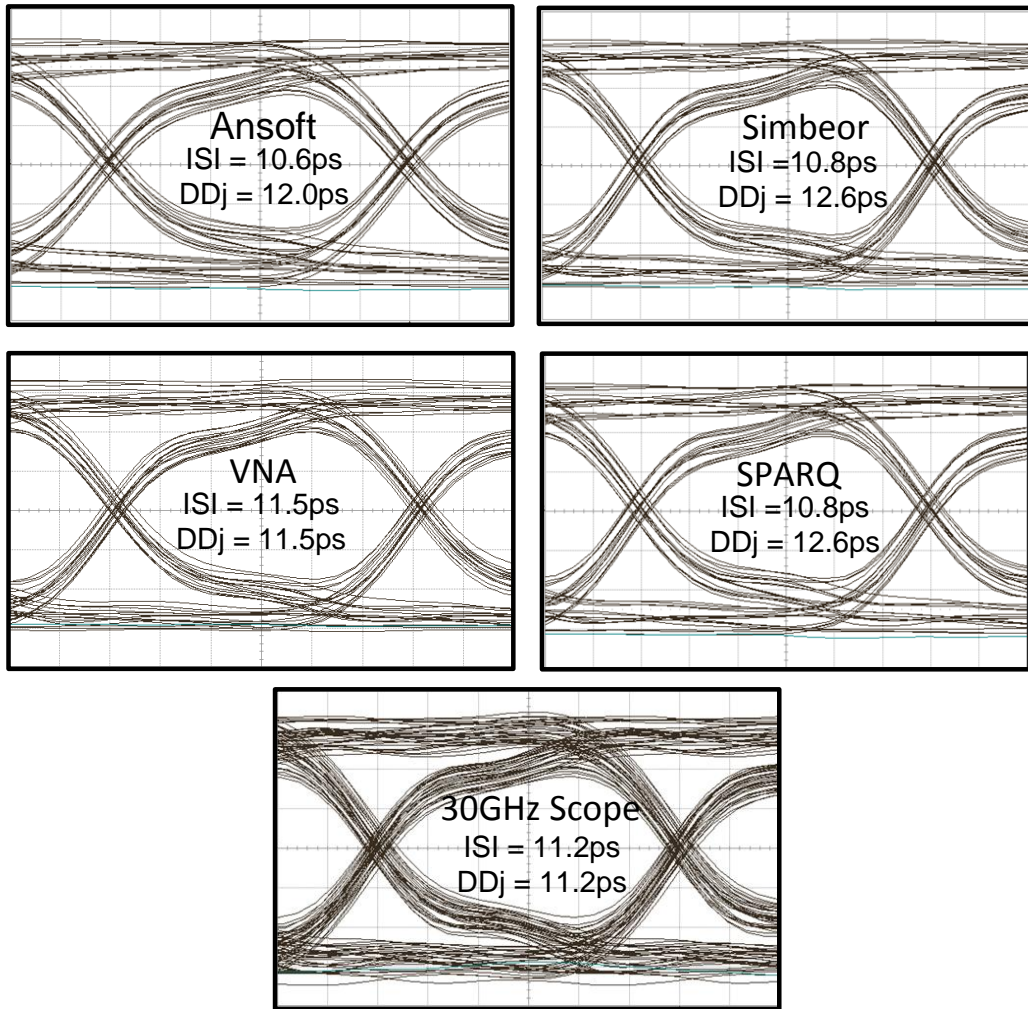


Figure 18 - 4 Co-simulations and 1 direct measurement of the “noiseless” eye-diagram for the 3” differential stripline structure, showing VERY good agreement between the deterministic jitter for all of these cases with measurement.

So far, so good. The same measurements and co-simulations were then performed on the 6-inch and 11-inch stripline structures.

6 inch Differential Stripline Comparison of Noiseless Eye Diagrams, ISI and DDj jitter figures.

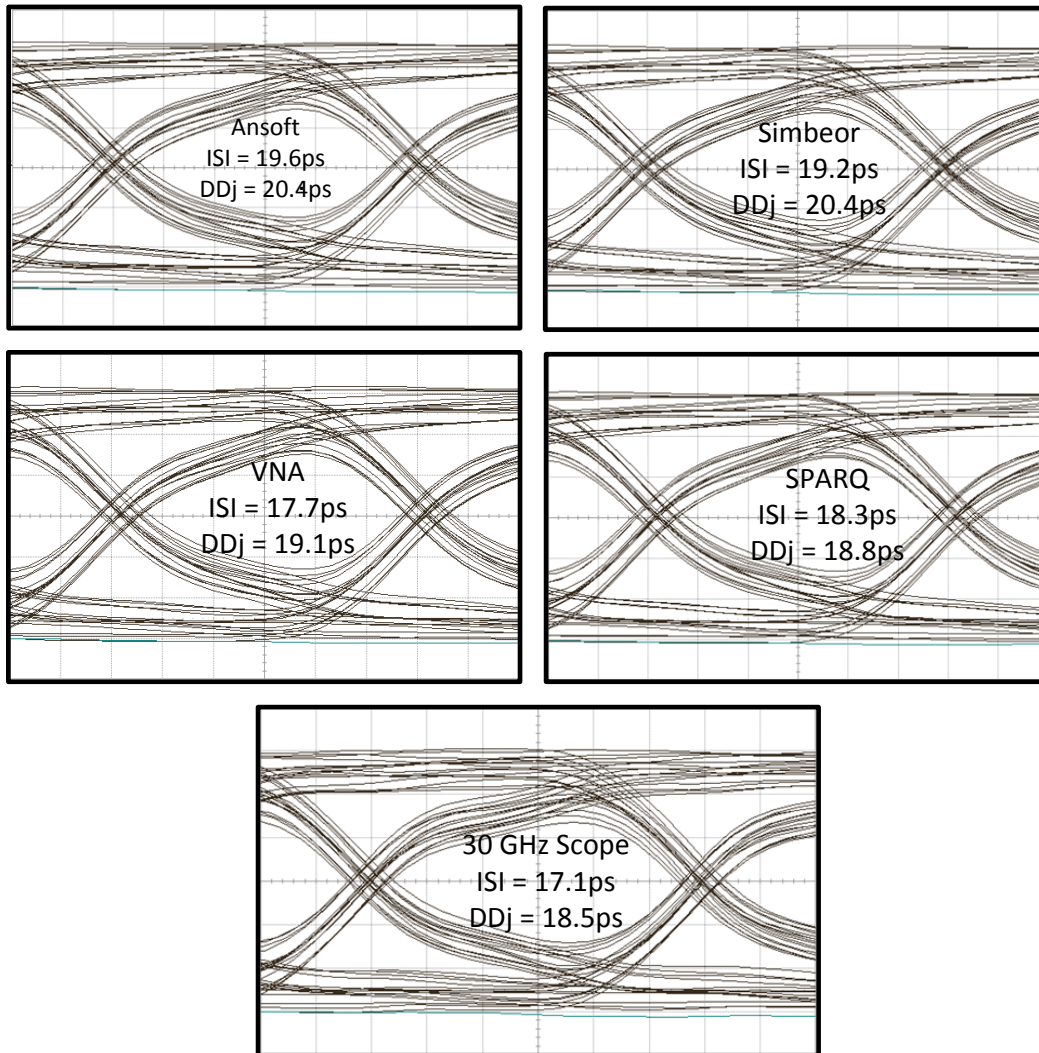


Figure 19 - 4 Co-simulations and 1 direct measurement of the “noiseless” eye-diagram for the 6” differential stripline structure, showing good agreement between the deterministic jitter for ALL of these cases with measurement and with each-other. (Note: the first printing of this paper showed a case which had poor agreement, which was corrected)

11 inch Differential Stripline Comparison of Noiseless Eye Diagrams, ISI and DDj jitter figures.

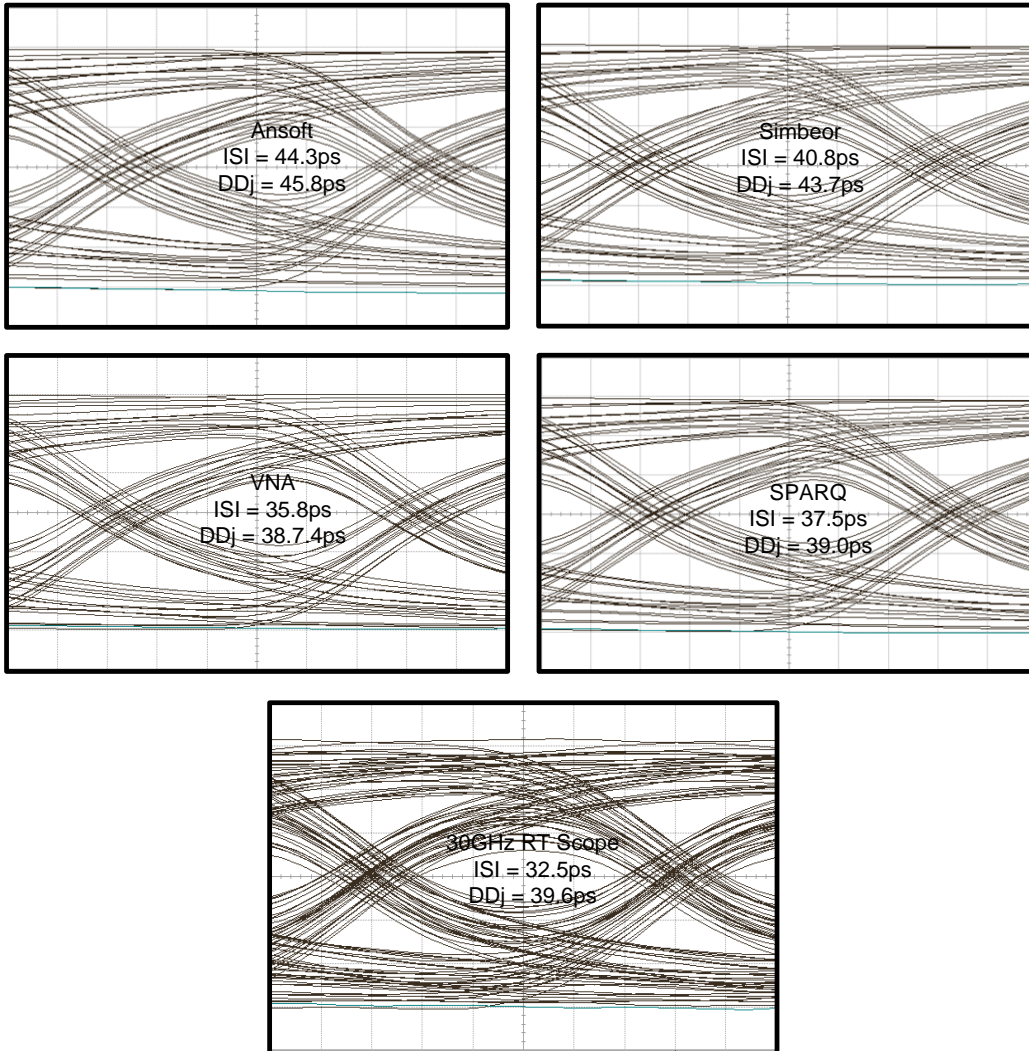
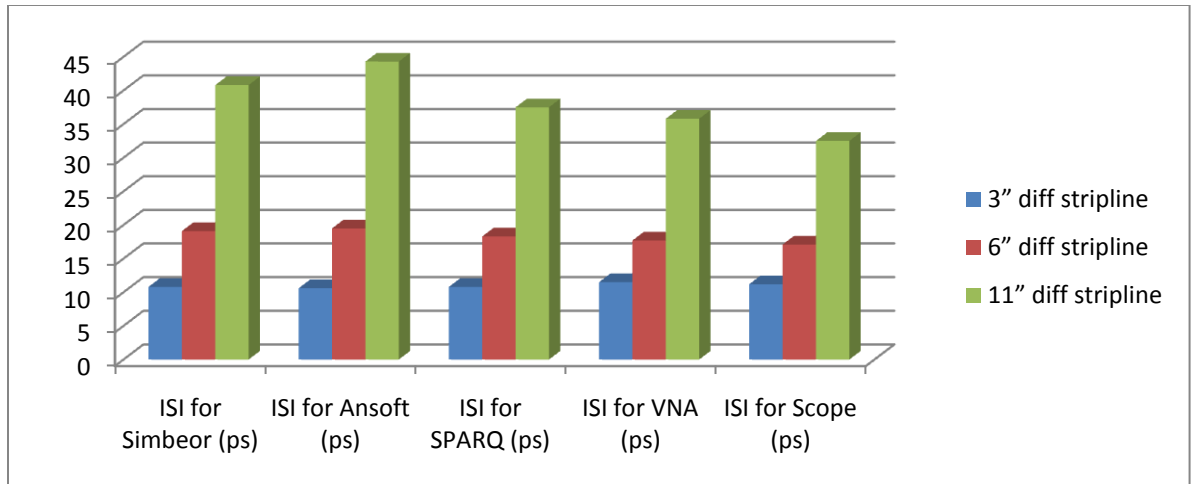
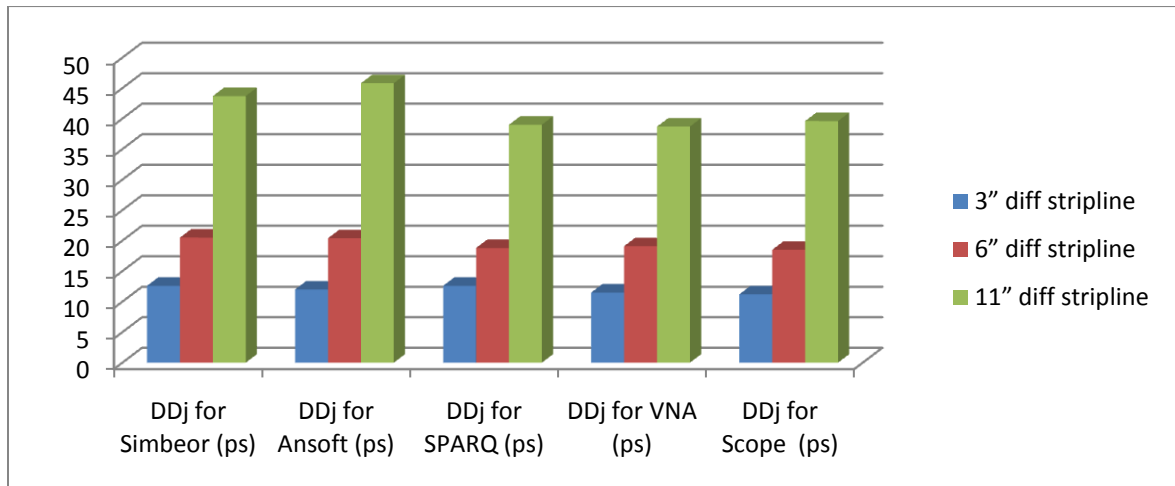


Figure 20 - 4 Co-simulations and 1 direct measurement of the “noiseless” eye-diagram for the 11” differential stripline structure, showing good agreement between the deterministic jitter for all cases based upon measurement (i.e. scope, VNA, and SPARQ/TDNA). The modeled values are consistently higher than the measured cases.



	ISI for Simbeor (ps)	ISI for Ansoft (ps)	ISI for SPARQ (ps)	ISI for VNA (ps)	ISI for Scope (ps)
3" diff stripline	10.8	10.6	10.8	11.5	11.2
6" diff stripline	19.1	19.5	18.3	17.7	17.1
11" diff stripline	40.8	44.3	37.5	35.8	32.5

Table 4 - : ISI values for 4 Co-simulations and 1 direct measurement of the “noiseless” eye-diagram for the 3”, 6” and 11” differential stripline structures, showing good agreement for all cases except for the 11” case.



	DDj for Simbeor (ps)	DDj for Ansoft (ps)	DDj for SPARQ (ps)	DDj for VNA (ps)	DDj for Scope (ps)
3" diff stripline	12.6	12	12.6	11.5	11.2
6" diff stripline	20.5	20.4	18.8	19.1	18.5
11" diff stripline	43.7	45.8	39	38.7	39.6

Table 5 - DDj values for 4 Co-simulations and 1 direct measurement of the “noiseless” eye-diagram for the 3”, 6” and 11” differential stripline structures, showing good agreement for all cases.

Note: The eye-diagrams for all of the measurements and Co-simulations for the baseline structures can be found in Appendix B: Oscilloscope Images.

To understand this comparison it is important to grasp the following facts:

- While the co-simulated (i.e. real input stimulus, but emulated channel) produces a much cleaner eye diagram than the measured eye-diagram, the systematic (ISIplot) noiseless eye-diagram looks very “believably” similar,
- The ISI values from the generator and those estimated for an ideal signal stimulus do NOT add linearly, since the value is a peak-peak for the entire distribution of crossing times, and there is no guarantee that the ISI of the generator is distributed in the same way as the channel. In particular “digital” crosstalk (a presumption on my part that this is the principle culprit) in the electronics does not look like a band-limited channel.
- The reader may also notice a lower level of “noise” in the co-simulation. It’s an important feature of emulation (applying the effect of a band-limited channel) that the noise bandwidth is reduced, and there is a lower level of noise at the output than at the input. In addition, when the real channel is present, the signal amplitude is reduced and typically the noise of the oscilloscope becomes more important. The oscilloscope’s bandwidth is open to a much wider band when observing the output of the channel as well as having intrinsic noise of its own.

Here are the measured cases for the 6” and 11” differential stripline cases.

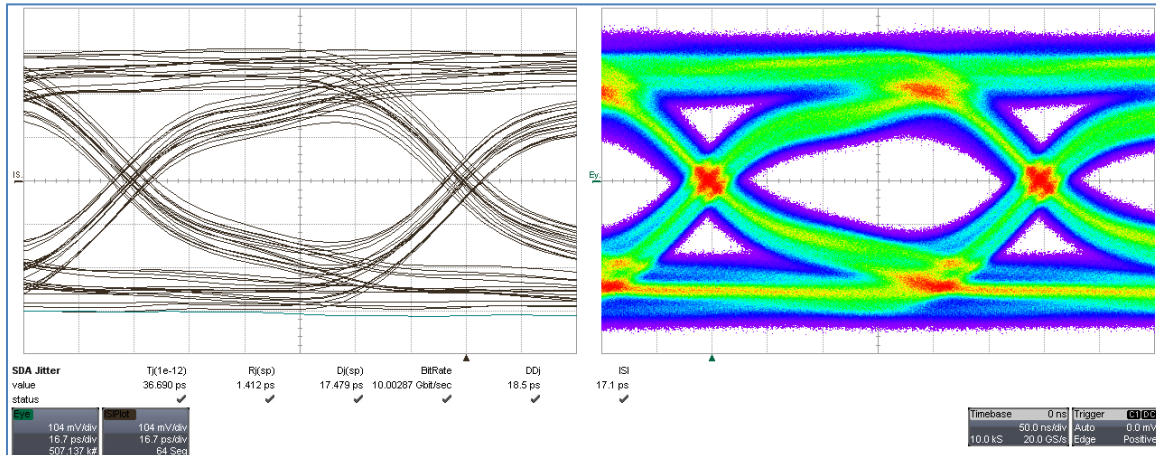


Figure 21 - Measured 6” differential stripline with cables de-embedded. Measured are 17.1ps ISI, and 18.5ps of DDj

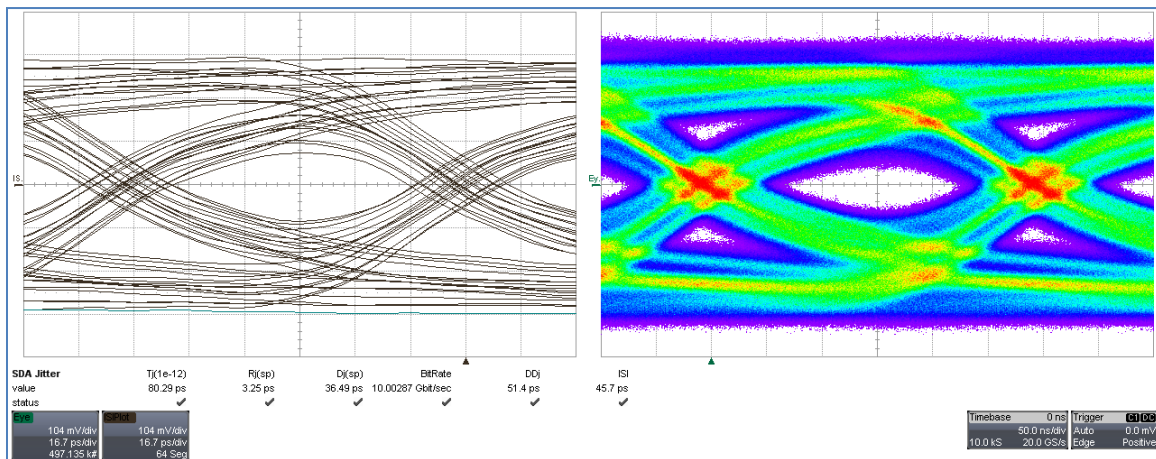


Figure 22 - Measured 11” differential stripline with cables de-embedded. Measured are 45.7ps ISI, and 51.4ps of DDj

Preliminary conclusions on baseline measurements:

For the 3” case, the correspondence for the jitter numbers is strikingly good for the co-simulations compared to measured values (with de-embedded cables, connectors and launches). The 6” case is still quite good, while the 11” case shows that the SPARQ and the VNA data begin to diverge from direct measurement, The SPARQ data is yielding about 10% lower ISI than the two 3D models. While the VNA data predicts nearly 20% higher ISI than the measurement and nearly 50% higher than the two 3D data sets.

Cross-talk Measurements and Models

During the prefabrication phase, the generators and oscilloscope were already available, and rather than using an idealized (virtual) signal source, the generator's signals could have been recorded and used in co-simulation. The biggest reason NOT to rely on this approach is that the virtual signal source was infinitely more flexible in terms of patterns and injected aberrations. In particular for the purposes of cross-talk, the variety of victim aggressor combinations was a boon to experimentation. For example: very fine control of the relative phase of the synchronous aggressor is possible without requiring a precise and calibrated variable delay element. Another reason that the simulated stimulus is desirable for the cross-talk cases, is that the 30GHz analog bandwidth oscilloscope that was available recorded only 2 channels of 80G samples/s. While it would have been possible to record on 4 channels at 16GHz with this particular oscilloscope, I decided that would be insufficient for a thorough treatment of the 10 Gb/s data signal. As such, I could not co-simulate with both an aggressor and victim which are phase locked. Neither could I invest the time to build a more sophisticated virtual stimulus (which I know is possible) to obtain a flexible aggressor which is phase locked to the victim.

Relatively content with the correspondence between actual measurement and prediction for the simple "baseline" structures, some experiments in crosstalk were performed. Many scenarios were studied, which only one such trial is described below.

The "McMorrow coupler" was designed to provide a 16-port crosstalk platform. As with our other aims, this was substantially more complex than we had time to thoroughly explore. However, it is already quite an interesting exercise to explore just one 8-port case (allowing for the assumption of perfectly terminated structures which are excluded).

It is possible to reduce a 16-port scattering parameter set to an 8-port set of parameters. The tools used in this case are internally developed tools (at LeCroy), but certainly other tools are available. Once equipped with an 8-port description, the simple 1 victim, 1-aggressor differential scenario is easy to simulate.

While cross-talk is sometimes discussed in terms of common-mode and differential-mode "coupling", another approach (and the one I have taken here) is to simply assert that the S-parameter set (single-ended or mixed-mode) completely describes the coupling between two differential pairs. In other words, to emulate the s8p system with the victim pair and aggressor pair associated with these ports (or something similar).

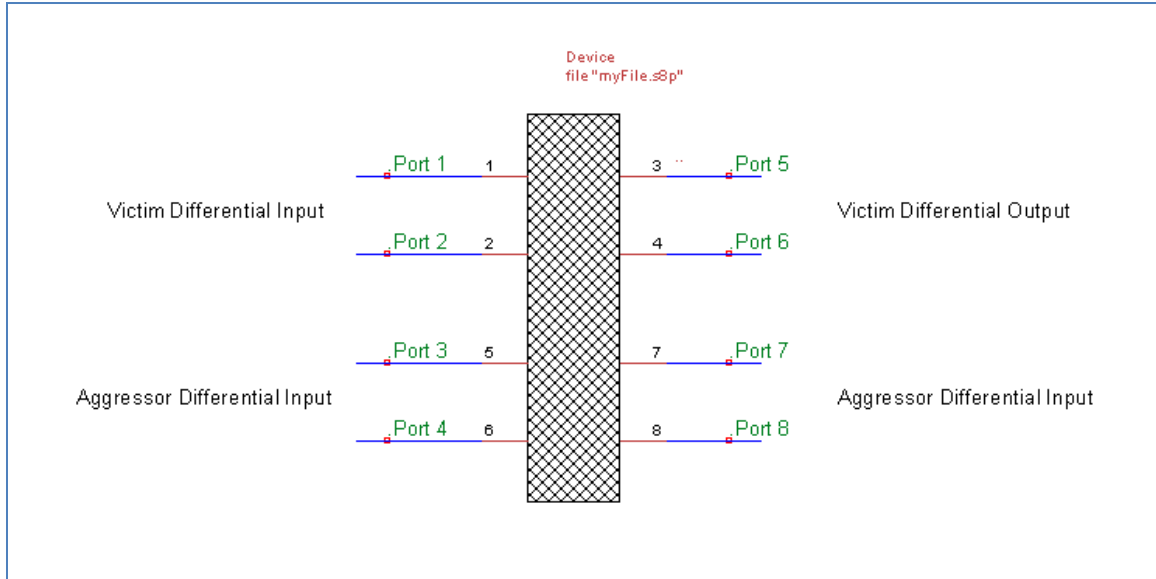


Figure 23 - Schematic of Victim-Aggressor configuration for an 8-port Scattering Parameter set.

Once so equipped, by providing stimulus for the victim and for the aggressor can provide measurements of the effect of the aggressor on the victim, or “cross-talk”. Such simulations are extraordinarily useful (compared to actual measurements) not only because they can be done “pre-fab” ... but also because simulation is vastly more flexible than what can be achieved with real generators and measurements.

Below is a simulation (post-material extraction) of S-parameters for one “broadside” case of the “McMorrow Coupler”. The first case (Figure 24) is the control case, or “no aggressors” case.

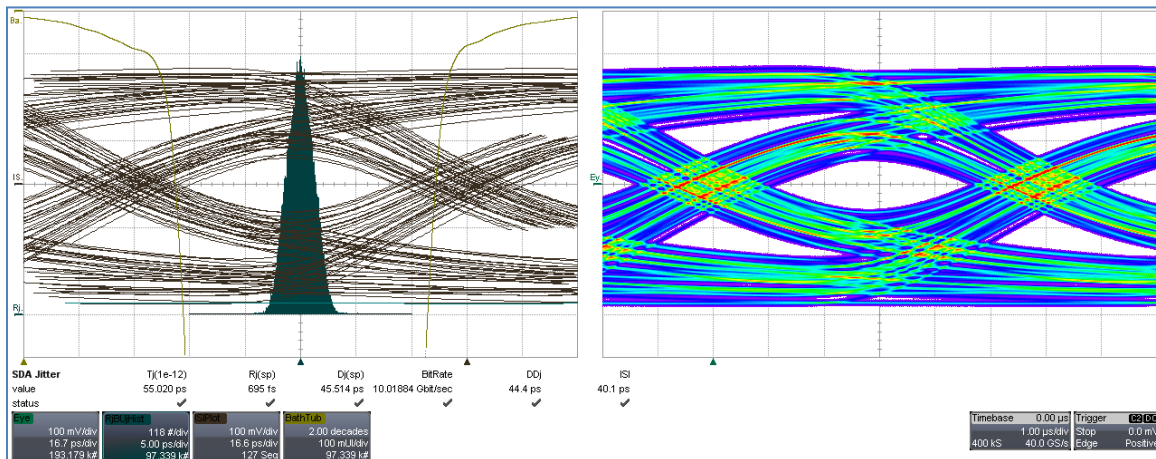


Figure 24 - A simulation of the “no aggressor” case for the long run of the McMorrow cross-talk stripline. “emulating” the channel using the reduced 16-port S-parameters from AnSoft 3D solver. The left frame shows the noiseless eye-diagram, the histogram of jitter (data-dependent effects removed) and the “BathTub” curve.

The entire simulation of the s8p structure was used, however the aggressor has no stimulus. This serves as the no crosstalk case. Then an aggressor was applied, and the

victim’s response observed. For this case, we used a PRBS31 data stream which was synchronous with the victim channel, but essentially “uncorrelated”.

It should be obvious that, were we to use the same PRBS7 for the aggressor, the effect would manifest as data dependent jitter, having the same effect on every bit of the PRBS7 sequence on the victim. That would not be a useful case. Likewise, a sequence which is “short”, like PRBS9 for example, would after some cycles of the pattern “resynchronize” with the victim pattern. It is our belief that such scenarios are not representative of cross-talk “in real-life”.

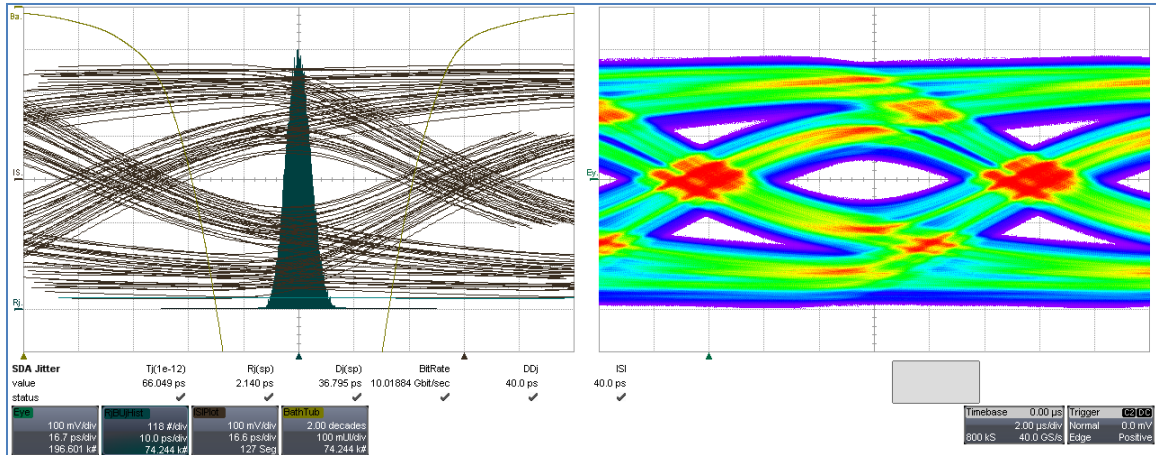


Figure 25 - A simulation of the PRBS31 synchronous aggressor case for the long run of the McMorro cross-talk stripline. “Emulating” the channel using the 16-port S-parameters from AnSoft 3D solver. The aggressor is on the “Broadside 2” differential structure. The left frame shows the noiseless eye-diagram, the histogram of jitter (data-dependent effects removed) and the “BathTub” curve.

Armed with this prediction, we move forward to an actual measurement of the cross-talk scenario. As for the simulation, a synchronous aggressor of PRBS31 is used.

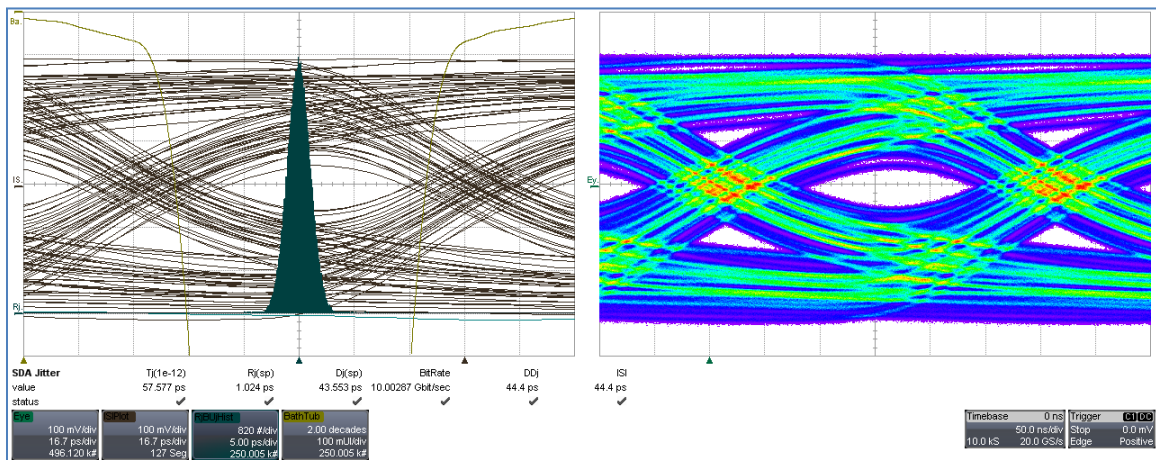


Figure 26 - Direct measurement of the victim differential pair for the “McMorro Coupler”. This is the “control” case, so the aggressor is “off”. The victim is a real generator PRBS7 and is measured with a real-time oscilloscope. Correlation with the simulation is excellent.

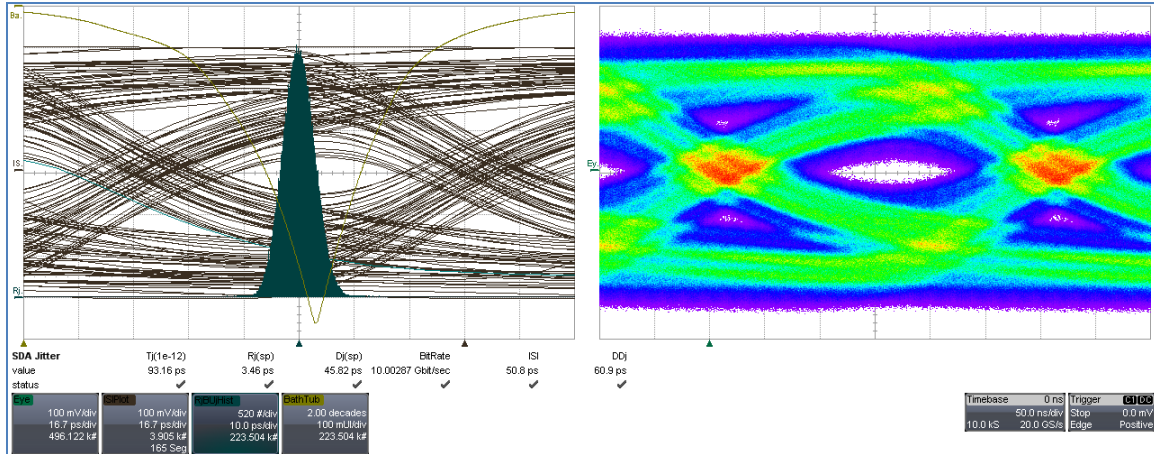


Figure 27 - Direct measurement of the victim differential pair for the “McMorrow Coupler”. The victim is PRBS7 and the aggressor is PRBS31 phase locked to the same clock, but at arbitrary phase. (Cables are de-embedded even though they are high quality)

While the control case is text-book “good correlation”, there is some reason that two things make less sense from when looking at this result.

1. Even in the simulation case, it appears the Rj for the aggressor-on case triples from about 700fs to 2.1ps. Likewise in the measured case the Rj triples. The absolute value of the Rj is not so important since the simulation source (NOT Co-simulation) has a setting which produces the lower control case number of 700fs). I believe this is due to a weakness in the assumptions used in the spectral Rj method, which in this case is incorrectly identifying the “wide-band” jitter produced by the PRBS31 aggressor as Rj.
2. The More surprising result is that the ISI and DDj numbers grow much larger for the cross-talk case than in the simulation. This is not expected, since these data dependent measurements are averages, and the Aggressor is in principle un-correlated. I fear, this may be due to the nearly closed eye of the measured crosstalk case. I believe this identifies an issue that must be addressed in the future (in the jitter extraction software).

A further experiment was performed, using this same measurement (waveform) data. In fact, it’s quite a practical experiment, since a reliable data channel with the kind of stress we observe and expect for the 11” stripline, some form of equalization is likely to be required. As such, jitter measurements for this case are perhaps more meaningful for the Neves Pathological.

For the following images, the spectrum of jitter is shown on the left. Notice that the cross-talk case has a much larger “background”. This accounts for the rise in Rj, although frankly it is not really Rj (since the cross-talk contributions are decidedly “bounded”). The cross-talk from the uncorrelated PRBS31 masquerades as background in the spectrum.

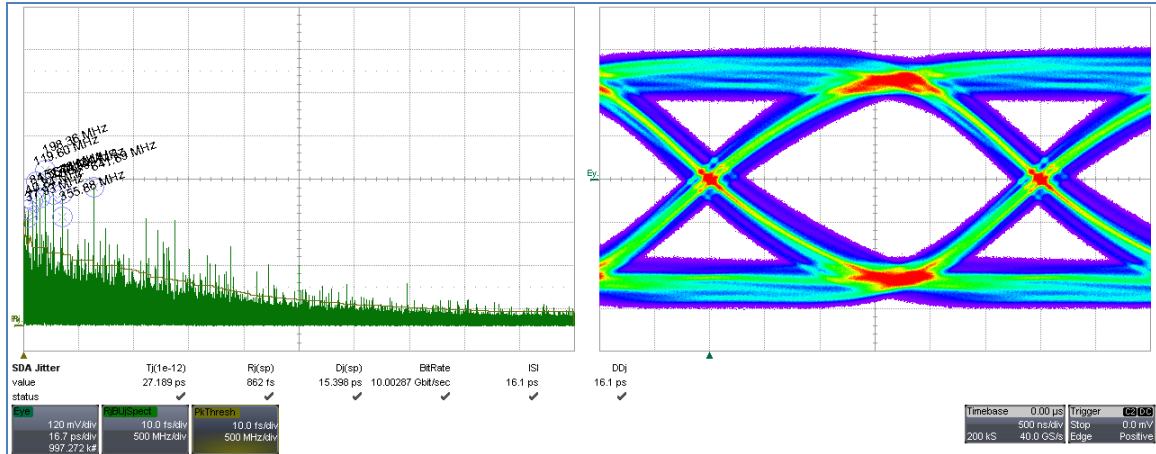


Figure 28 - Using an FFE equalizer to open the eye, the jitter and eye diagram can still be calculated for (McMorrow) simulation. This is the control or “no aggressor” case, and it is a simulation.

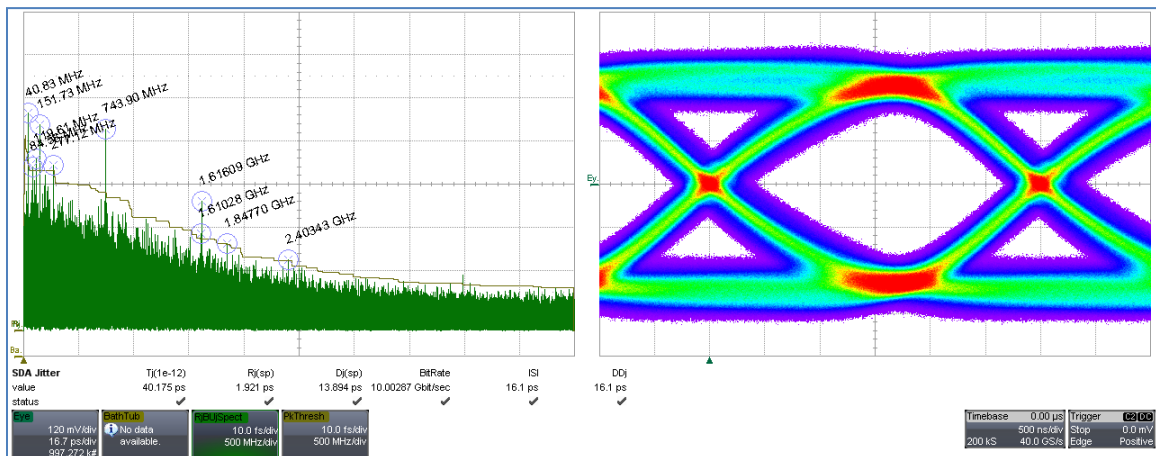


Figure 29 - Using an FFE equalizer to open the eye (same tap values), the jitter and eye diagram can still be calculated. Synchronous PRBS31 aggressor (McMorrow). This is a simulation of the “aggressor-on” case. Note the ISI and DDj do not increase ... which is expected since they are systematic. Note also that the Rj value increases by about a factor of 2.

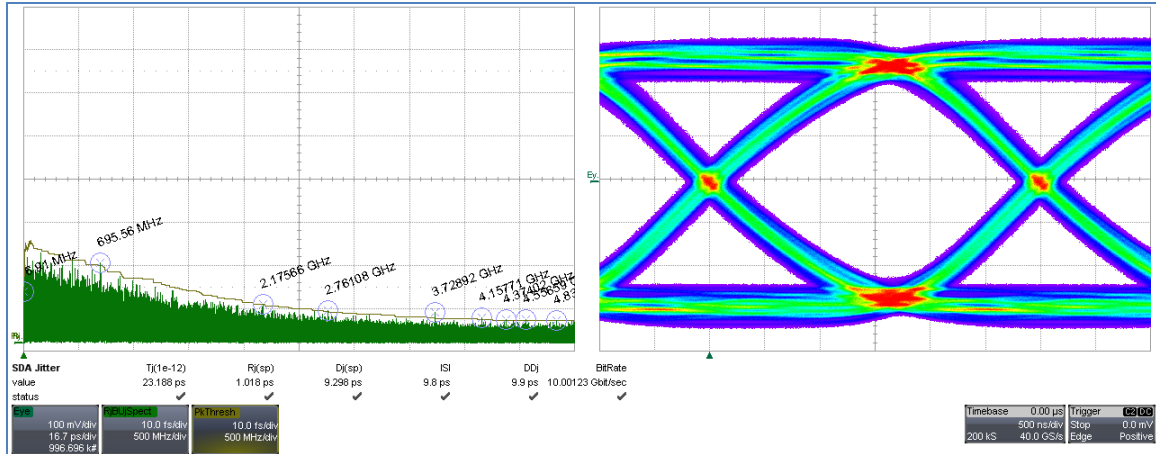


Figure 30 - Measurement of PRBS7 Victim ... FFE 5 taps, 2 pre-cursor, as for simulations above. This is not a simulation. It is the control case (no Aggressor). Approximately 1 million UI.

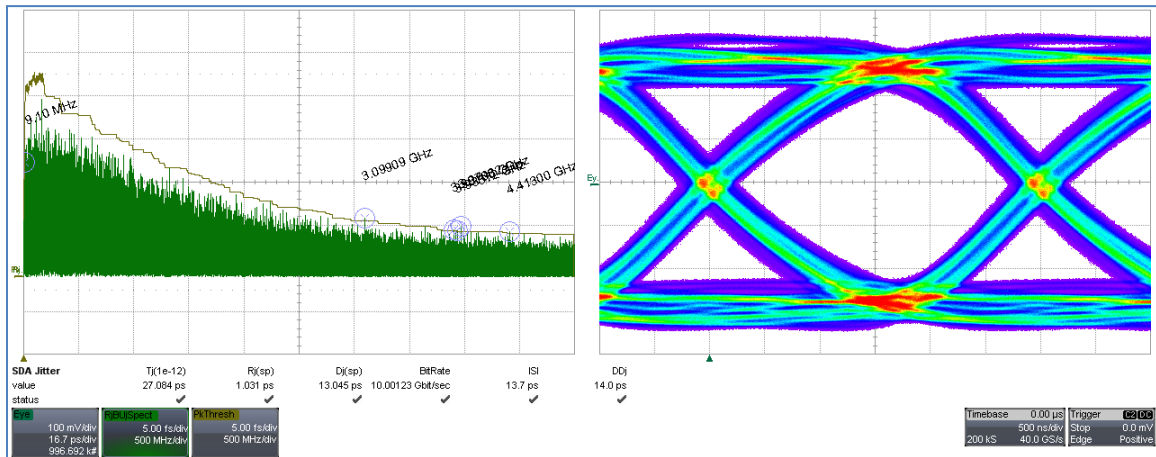


Figure 31 - Measurement of PRBS7 (by accident) Aggressor, with a PRBS7 Victim ... FFE 5 taps, 2 pre-cursor, as for simulations above. Note the Rj unexpectedly did not grow with the cross-talk case.

Now there is a mystery here, and it took days to find it: Using another tool, the crosstalk was analyzed to identify a phase dependency in the vertical noise of the victim channel. Figure 32 shows the vertical noise for every UI of the data pattern as a function of phase within 1 unit interval. Exactly on the same horizontal scale as the eye diagrams shown here. This indicates the phase of the Aggressor relative to the victim. The same plot for the measured data (for the data set presented here) does not exhibit this behavior ... it is perfectly uniform. So, the Aggressor was not synchronized as I believed it to be when measuring. It was for several other cases, and those will be added to the paper as well as a re-measurement of this case.

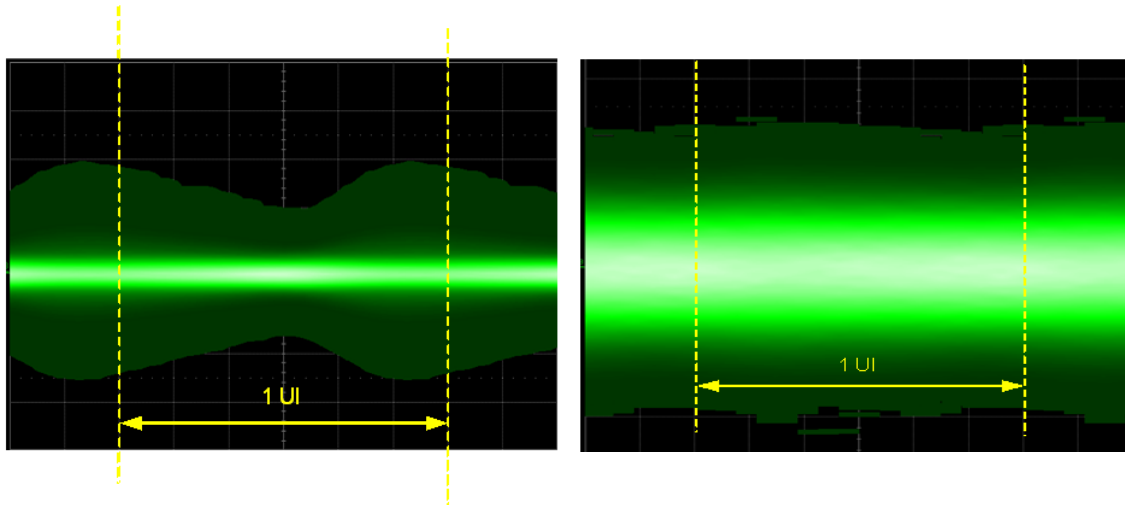


Figure 32 - Display of the phase dependent noise (left) on the victim channel for the PRBS31 Aggressor and PRBS7 victim simulation . This display is “flat” for the control cases (right), and merely inflated for the Measured cross-talk case, indicating that the Aggressor channel was not phase locked, as it was believed for the measurement case (while the aggressor was certainly synchronized for the simulation case). Vertical scale is note the same.

It was discovered that the aggressor generator was *incorrectly* set to PRBS7 pattern (a consequence of someone borrowing one of the generators and retuning it with a different jumper setting).

You might ask: why include this example in the paper? It was not the intention of the experiment to measure with an aggressor signal which is “coherent” with the victim signal. However, it is a useful example of why using the same aggressor pattern as the victim pattern is *NOT* a useful test case.

After realizing this error, it’s obvious why the ISI and DDj increased, or at least changed. The effect of the “coherent” but random fixed-phase aggressor is to change the shape of the signal under test, in a completely pattern dependent way. That explains also why Rj did not grow in this case. (It stayed the same at approximately 1ps).

The following is a do-over for this measurement using a properly synchronized PRBS13. It is a different generator (because access to the original generator was not possible), and it has considerable spectral structure (much more than the original victim generator), so try to ignore that difference.

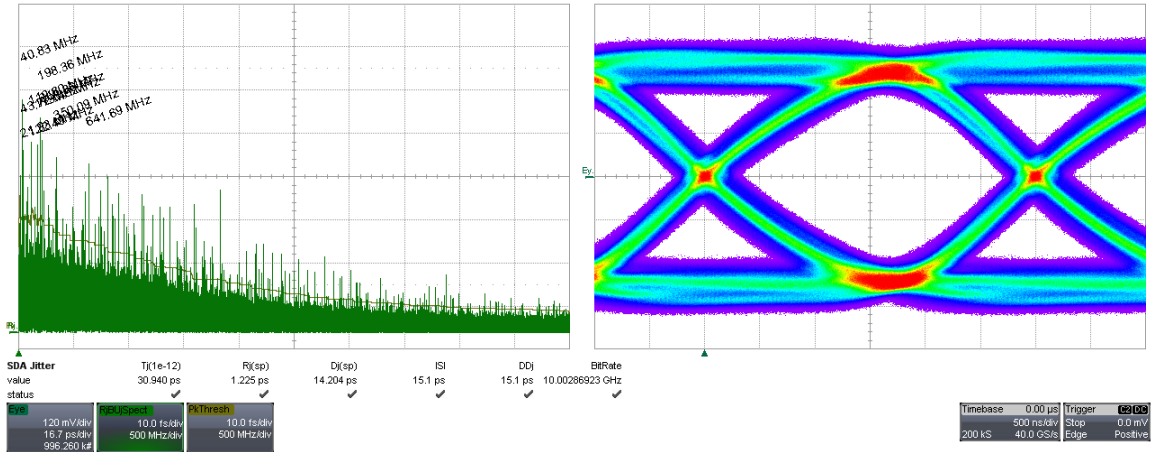


Figure 33- Measurement of No Aggressor, with a PRBS7 Victim ... FFE 5 taps, 2 pre-cursor, as for other cases which are equalized above. The Rj is 1.23ps, and is slightly larger than the 1ps Rj for the original PRBS7 generator.

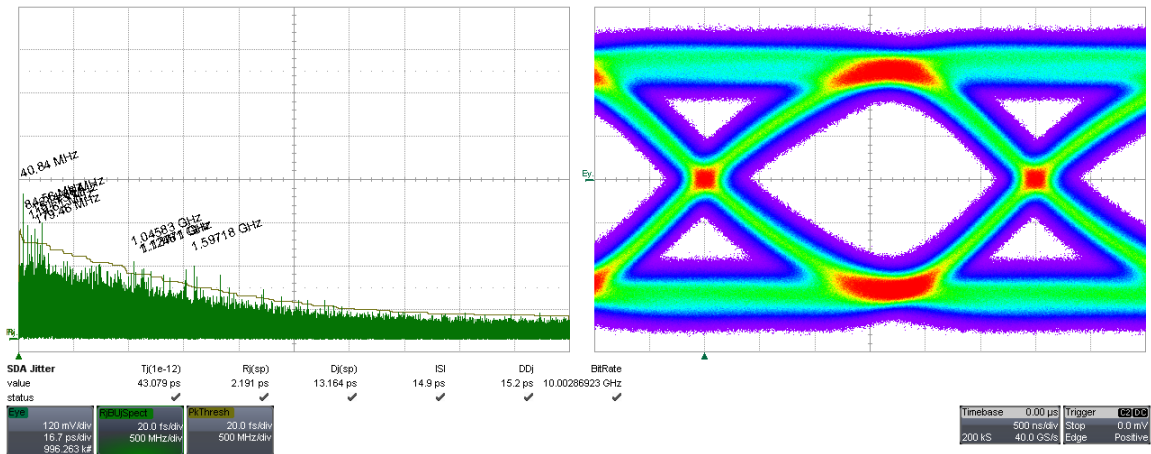


Figure 34 - Measurement of synchronous PRBS31 Aggressor, with a PRBS7 Victim ... FFE 5 taps, 2 pre-cursor, as for other cases which are equalized above. The Rj does increase, and by about a factor of 2, like it did for the simulation of equalized data.

The repeat of the measurement shows much better agreement with the simulation. And the random jitter increases by a roughly factor of 2. Again, this is (I believe) attributable to the incorrect assumption of the “Spectral Method” of Rj extraction, that the “background” of the jitter spectrum represents the effect of Rj. In this case, the background contains a large component of bounded jitter that is very broad-band, and so contributes to background.

Conclusions

Perhaps the first and most significant conclusion is that the test board designed and fabricated for this paper provides a host of information and more structures than we could possibly treat in one paper. We fully expect to produce more results from this platform.

Concerning Estimating Jitter from Pure Models

We learned several lessons during this exercise. We learned that the data pattern chosen for estimating DDj and ISI as well as the shape of the predicted eye-diagrams is very important. These deterministic jitter figures are strongly dependent on the data pattern used for a stimulus. We also learned that care must be taken in performing channel emulation, to maximize the duration of the impulse (or filter) response of the process. Finally everything made sense, but it was not without effort to attend to every detail.

Concerning material properties

A test board for material parameters identification and simulation to measurement validation was designed, manufactured and validated for this paper. The board was used for the material identification and post-layout jitter analysis in coupled differential channels. We observed relatively large variations of the dielectric parameters on the test board.

Use of coupled line GMS-parameters for material identification was outlined and validated in the paper. We have shown that GMS-parameters of coupled lines in inhomogeneous dielectric have 2 unique parameters that can be used to detect the dielectric inhomogeneity and to identify or validate parameters of two dielectrics simultaneously. It was shown that correct identification of material parameters for layered dielectrics is important for the analysis of isolated and coupled differential nets.

A statistical model of dielectric or model dependent on the trace routing angle may be required for exhaustive compliance analysis of interconnects on such dielectric. Dielectric model with anisotropy in the XY-plane (board surface plane) may be alternative to the angle-dependent solution. All fixtures on our test board were in two dielectrics with unknown properties. That complicated the identification process and introduced some ambiguities in the identification results even with the coupled lines. Single-ended microstrip structures without solder mask could be used for unique identification of the prepreg (or core) layer first to avoid the ambiguity of the identification of two dielectrics simultaneously.

Concerning VNA and TDNA and Scope Measurements

A number of lessons were learned. First we learned that it is essential to perform “baseline” measurements on simple structures (both network analysis and channel measurements). Not only are these simple measurements essential to the material issue just mentioned, they are essential to build confidence and familiarity in the basic use of the measuring instruments. After all, if you can’t get past confirming the s-parameters, eye diagrams look as predicted and the most simple jitter measurements make sense (of which the ISI and DDj measurement are among the most basic), then how can you proceed to the tricky cases of multi-lane cross-talk.

When using a variety of instruments such as we have here, it was no small part of the effort to correlate and compare the results to simply keep straight the differences in “conventions” regarding S-parameters. It seemed at first that every one of the 5 authors had a different presumed numbering of ports, or a preference for single-ended or mixed-mode S-parameter views. Much time was spent working out how to re-order ports from all of our measurements and modeling tools. Also in dealing with these data sets, one encounters a broad interpretation of the “touchstone” file standard. The lesson here is: be prepared for attention to detail.

Another lesson learned in this process was to be sure of the quality of cables and connectors. If the intention is, as it was for our measurements, to “de-embed” the cables, launches and connectors, then they cannot be too lossy. The de-embedding or removal of the effect of an element in the measurement is only feasible if you are correcting for too much. You can compensate a 6dB loss with a penalty in noise, but much beyond that you are in dangerous territory.

An important lesson is that signal sources used for these kinds of measurements (like all electronic instruments) are not perfect. For more accurate predictions, the simulations (in particular for the deterministic jitter measurements) need to include the imperfections in the generated stimulus. One way to do this is “Co-simulation” as we have done here.

The biggest lesson learned concerning these basic measurements is that the tools pretty much work. You can predict the jitter and eye-shape from the 3D modeling tools. The better your materials estimates are, the better the prediction will agree with measurement. We can say, the deterministic jitter predictions are well within expectations, including the 11” stripline. (*While the initial printing of this paper showed an outlying case for the VNA results, a correct treatment of the measurement data yielded excellent correlation*).

Concerning Jitter and Cross-talk measurements

As for the jitter measurements, one conclusion is that as the signals under test become severely stressed, the jitter results become less reliable. In particular, the channel chosen as the victim for the McMorrow structure is lossy. In the presence of crosstalk, the eye becomes nearly closed and it is difficult to perform the decode to remove DDj. One conclusion is that this case needs to be handled in a more robust way. In particular it’s a subject of great interest whether we should even discuss “jitter” for a very closed eye, or if we should treat such cases with the equalization that would be required for a more reasonable transmission?

There are a large number of cross-talk structures on this test board. For the McMorrow coupler case, the model and measurement are in agreement about one thing: that for the equalized case and for the un-equalized case, R_j appears to grow by an unexpected amount. The case under study of the PRBS31 aggressor produces an effect in the spectrum of jitter that is not easily identified as “bounded” jitter. There are statistical

methods for extracting R_j (see Appendix B ref 8) but they require very large statistical samples, and for this case large compared to 2 to the 31st power.

Also in disagreement, and requiring further study, is why the coupling and structure of the effect of the aggressor for this case is not as marked as it is for the simulated (S-parameter based) estimation of the cross-talk. More investigation needs to be made into both of these issues.

Closing

It has definitely been a positive experience to work in a group as we have here. It has not always been easy, but it has been fruitful. The benefit of the multiple areas of expertise and many years of experience among us has made this effort very satisfying and enlightening.

The test board produced for this paper contains many interesting structures that were not even mentioned in this paper. These structures will be the subject for further investigation and iterative refinement of the board design and material parameters extraction methodology as well as jitter and cross-talk phenomena.

Appendix A: Material Parameters Identification

Design of interconnects for 8-10 Gb/s applications requires electromagnetic models validated in the frequency range from DC up to 20-25 GHz. Characterization of composite dielectrics from DC to 20-25 GHz for such analysis is the particularly challenging task – a review of the recent publications on the subject is available in [1]-[2]. **Meaningful multi-gigabit interconnect design and compliance analysis must start with the identification of the dielectric properties over the frequency band of interest.**

In paper [2] a simple practical procedure for extraction of dielectric parameters on the base of generalized modal S-parameters (GMS-parameters) was suggested. Since then, the technique has been successfully used on multiple prototype and production boards such as PLRD-1 [2] or CMP-08 test board featured in this paper. The material identification method is based on comparison of the GMS-parameters extracted from the measured data with GMS-parameters computed for a line segment without launches or connectors. The key in such comparison is the minimal number of the parameters to match. Only generalized modal transmission parameters are not zero and are used for identification. Both computed and measured generalized reflection and modal transition parameters are equal to zero exactly. It simplifies the identification process a lot without sacrificing the accuracy and make the GMS-parameters method the simplest possible. It does not require multiple structures for broad-band TRL calibration and expensive 3D full-wave modeling of launches and connectors. Just two segments of line of any type and with any characteristic impedance and launches can be used to identify dielectric properties. Theoretically, no optimization or modeling of the launches from probes or coaxial lines is required. Practically, the connector choice and launch design are important, because of the insertion loss of the test fixtures for the material identification should stay within the dynamic range of the measurement equipment. It means that the connectors should be selected and the launches are designed with the goal to avoid the transmission resonances that can severely degrade the material identification accuracy. Thus, some preliminary electromagnetic analysis and optimization are typically required as we will show in this paper.

PCB dielectrics are inhomogeneous, usually a mixture of glass and epoxy that can be characterized either as the mixture of two models or, more often, with an effective dielectric model. Space between traces in coupled microstrip lines may be filled with the solder mask with dielectric properties different from the substrate dielectric. In addition, prepreg and core layers in strip-line configurations may have different dielectric properties. Space between traces in coupled strip lines may be filled with epoxy only or even with air depending on the manufacturing technology. Use of one effective dielectric model may be not accurate enough for analysis of coupled lines and for the cross-talk analysis. For accurate characterization of coupling effect we may need to identify and use parameters of at least 2 dielectrics (preferable, more accurate model) or use one anisotropic dielectric model in case of strip lines. **We show here how to use GMS-parameters of coupled lines for identification of material properties suitable for accurate simulation of multi-gigabit signals in differential and coupled interconnects**

up to 20-25 GHz. Identified dielectric models will be used to validate analysis with the measurements for different coupled differential structures.

Let's start with the definition of the generalized modal S-parameters (GMS-parameters) for coupled (or differential) transmission lines. GMS-parameters of a coupled line segment is a 4 by 4 complex matrix with very simple structure:

$$GMSc = \begin{bmatrix} 0 & 0 & \exp(-\Gamma_1 \cdot dL) & 0 \\ 0 & 0 & 0 & \exp(-\Gamma_2 \cdot dL) \\ \exp(-\Gamma_1 \cdot dL) & 0 & 0 & 0 \\ 0 & \exp(-\Gamma_2 \cdot dL) & 0 & 0 \end{bmatrix} \quad (A.1)$$

Here dL is the length of the line segment, and $\Gamma_n(f) = \alpha_n(f) + i \cdot \beta_n(f)$, $n = 1, 2$ are complex propagation constants of two modes in the coupled line (even and odd for instance). **The most attractive and useful property of GMS-parameters of coupled lines (A.1) is simplicity – only 2 unique non-zero elements and independence of the characteristic impedance.** GMS-parameters can be directly computed from one side and extracted from S-parameters measured for two line segments on the other side. This is the basis of the material identification procedure suggested in [2] and refined here. Here are the five steps of the dielectric identification procedure (Simberian's patent pending):

1. Measure S-parameters of two test fixtures with different length of line segments S1 and S2;
2. From S1 and S2 compute GMS-parameters of the line difference (A.1)
3. Select material models and guess values of the model parameters
4. Compute GMS-parameters of the line difference segment (A.1)
5. Adjust material parameters until computed GMS-parameters fit measured GMS-parameters

Alternatively, the complex propagation constants can be used for the fitting step 5, that is practically equivalent to GMS-parameters.

Step 1. GMS-matrix of a line segment can be extracted from the measured S-parameters of 2 line segments with the length difference equal to dL . Following the procedure described in [2], we measure 4-port S-parameters for 2 differential transmission line segments with VNA or TDNA. S-parameters should be pre-qualified first and have reciprocity and passivity quality measures above 99% (see more on quality metrics in [7]). Theoretically, reflection from the connectors or launches does not matter for this method – the only requirement is the identity of all 4 launches. Non-identity should be within 2-3 Ohm for the identification up to 20 GHz (see more on that in [6]). Practically, the measured transmission parameters must stay within the dynamic range of the measurement equipment. The calibration is also optional here because of the identification procedure is self-calibrated. Let's assume that we measured two S-parameter models: S1 for the fixture with continuous coupled line segment L1, and S2 for the fixture with the continuous line segment L2.

Step 2. Following the procedure described in [4] we convert S-parameters into scattering T-parameters T1 and T2. As it was shown in [2], generalized modal T-

parameters (GMT-parameters) of the line segment difference can be expressed as the eigenvalues of the product of T1 and inversed T2:

$$GMT = \text{diag} \left[\text{eigenvals} \left(T2 \cdot T1^{-1} \right) \right] \quad (\text{A.2})$$

or:

$$GMT = \begin{bmatrix} T_{11} & 0 & 0 & 0 \\ 0 & T_{22} & 0 & 0 \\ 0 & 0 & T_{11}^{-1} & 0 \\ 0 & 0 & 0 & T_{22}^{-1} \end{bmatrix} \quad (\text{A.3})$$

Due to the reciprocity, there are only 2 unique elements in the GMT-parameters (A.3). Conversion of the GMT-parameters to GMS-parameters is straightforward and gives us measured GMS-parameters with just 2 unique non-zero elements:

$$GMSm = \begin{bmatrix} 0 & 0 & T_{11} & 0 \\ 0 & 0 & 0 & T_{22} \\ T_{11} & 0 & 0 & 0 \\ 0 & T_{22} & 0 & 0 \end{bmatrix} \quad (\text{A.4})$$

Here T_{11} is generalized transmission parameter for mode 1 (even for instance) and T_{22} is generalized transmission for mode 2 (odd for instance). The measured generalized modal transmission parameters in (A.4) should correspond to the computed values defined in (A.1) and this is the basis for the material identification method. Note, that the measured GMS-parameters may appear as noisy. It happens mostly due to non-identities of the investigated lines in two test fixtures, non-identities of the connectors and launches and due to discontinuities (if not straight lines are used). Note that the complex propagation constants of two modes can be easily computed from T_{11} and T_{22} and used for the identification, though this step is not necessary here. Measured GMS-parameters can be additionally fitted with a square root of frequency and polynomial functions to get rid of the small non-identity and measurement noise. Though, large non-identities lead to extremely noisy and distorted GMS-parameters that cannot be improved or used for the identification [6]. Thus, the extraction fixture must be always prequalified for the identification with TDR for instance. Note, that further post-processing of (A.4) with the goal to extract complex propagation constants and further the properties of the dielectrics from the attenuation and phase constant looks like a good idea at first, but in reality such methods are typically based on closed-form expressions for the attenuation and phase constant. Expressions allow separation of polarization and conductive losses, but the results of such extraction are not accurate due to multiple assumptions in the closed-form expressions that lead to over-simplification of the problem.

Step 3. As it was shown in [2], the wideband Debye (or Djordjevic-Sarkar) model provides good correlation for PCB dielectrics with relatively high losses. The model can be used in different software tools can be described with dielectric constant and loss tangent defined at one frequency point. Just one point defines causal analytical dependency of the complex dielectric constant from frequency.

Step 4. Using the dielectric model defined in Step 3, compute the GMS-parameters of the line segment (A.1). The propagation constants in (A.1) are frequency dependent in general and have to be computed by solving the Maxwell's equation for a cross-section of

the transmission line or extracted from 3D EM analysis of a line segment with the simultaneous diagonalization method [2] implemented in Simbeor software [3] is used in this paper. Only full-wave transmission line models with the causal dispersive models of dielectrics and conductors is suitable for the identification of material properties up to 20-25 GHz. Use of approximate microstrip or strip line models should be avoided because it introduces additional errors due to low accuracy of such models at high frequencies in general. Analysis with a static field solver can be used for the identification, but the bandwidth of such models are usually restricted to 3-5 GHz for PCB and packaging application due to low-accuracy modeling of dielectric and conductor effects and complete absence of high-frequency dispersion modeling. The results of identification with the static models may be considered only as a crude low-frequency approximation. Note that the appropriate conductor roughness model is also essential for the identification of the polarization losses.

Step 5. We first match the computed phase or group delay of the generalized modal transmission coefficients (A.1) to the measured values (A.4) by varying only dielectric constant in the wideband Debye model and re-simulating the line segment. After the phase and group delay are matching with sufficient accuracy, the next step is to adjust the dielectric model loss tangent to have magnitudes of the computed generalized modal transmission coefficients (A.1) matching the measured values (A.4). Technically, matching generalized insertion loss is equivalent to matching the attenuation part of the computed and measured complex propagation constants. Matching of the phases of generalized transmission parameters is equivalent to matching of the phase constant parts of the computed and measured complex propagation constants. **The final dielectric model is the one that produces the best match between computed and measured GMS-parameters or between computed and measured complex propagation constants.** Such model should produce expected correlation in the analysis of interconnects within reasonable variations of geometry of the traces.

The outlined material identification technique with GMS-parameters is the simplest possible for interconnect applications and the reasons are as follows:

- Needs un-calibrated measurements for two transmission line segments with any geometry of cross-section and transitions
- No de-embedding of connectors and launches (difficult, error-prone)
- Needs the simplest numerical model
 - Requires computation of only propagation constants
 - No 3D electromagnetic models of the transitions
- Minimal number of smooth complex functions to match
 - One parameter for single and two parameters for differential
 - All reflection and modal transformation parameters are exactly zeros

Before the material identification on CMP-08 board, let's analyze quality of the S-parameters measured for 3, 6 and 11 inch coupled line test fixtures or pre-qualify them. S-parameters measured up to 40 GHz are shown on the left plots in Fig. A.1 for microstrip test fixtures and Fig. A.2 for strip-line test fixtures. Passivity quality measures of all S-parameters were above 99.9% and reciprocity quality measures were above

98.8% that is acceptable [7]. All elements of S-matrix are above the noise floor below 25 GHz as we expected from the pre-layout analysis and optimization. VNA measurements had small problem below 100 MHz that was fixed by eliminating of those frequency points from the analysis and by use of interpolation to DC. Measured S-parameters of all models were fitted with the rational macro-models with RMS error smaller than 0.03. It means that the overall S-parameter model quality is above 97% that is typical for the measured data. S-parameter model with 40 GHz bandwidth allowed us to compute TDR profiles for all structures with high precision using rational macro-models. TDR profiles are shown in Fig. A.1 for all coupled microstrip structures, and in Fig. A.2 for all coupled strip line test fixtures used for the material identification. We can see relatively large variations of the impedance both in microstrip and strip line structures. This can be explained by different orientation of the line segments relatively to the fiber glass structure or by adjustments of some trace width by the board manufacturer. 3 in coupled line have different routing angle comparing to the 6 in and 11 in coupled line segments both for microstrip and strip line sections. Effective dielectric constant depends on that orientation that is clearly visible at the impedance profiles. Note that capacitive sub-optimal launches with a large dip on TDR profile around 0.3 ns were not a problem in the target frequency range. The SMA connector cut-off frequency was also above 25 GHz. Though, extension of the frequency range up to 40-50 GHz, for instance, would require selection of a different connector and iterative launch refinement. In addition, to stay in the dynamic range of the measurement equipment, the lengths of the lines used for the material identification should be reduced or, alternatively, dielectric with lower losses should be used.

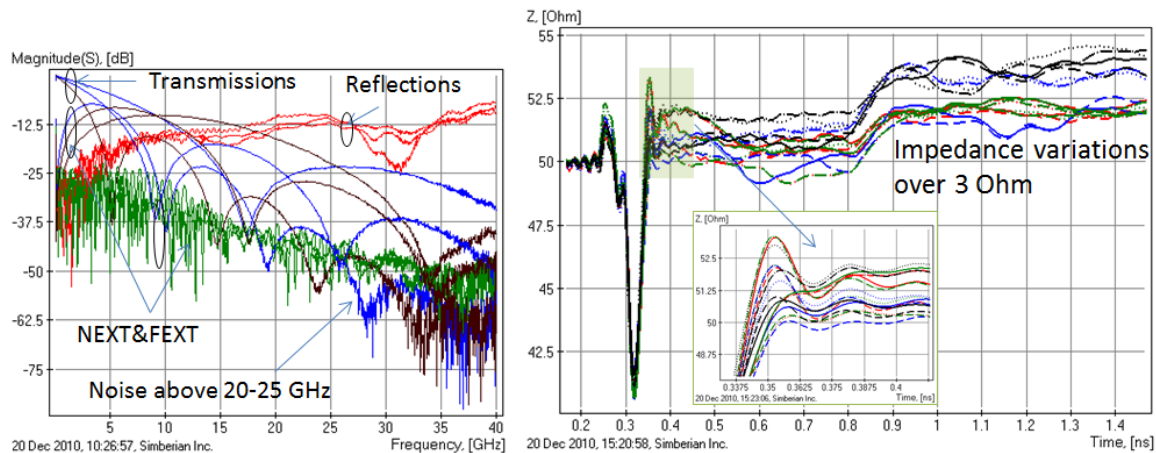


Fig. A.1. Measured single-ended S-parameters for 3 test fixtures with coupled microstrip line segments (left graph, parameters in the first row of S-matrix are shown); TDR profile for all coupled strip line structures (right graph).

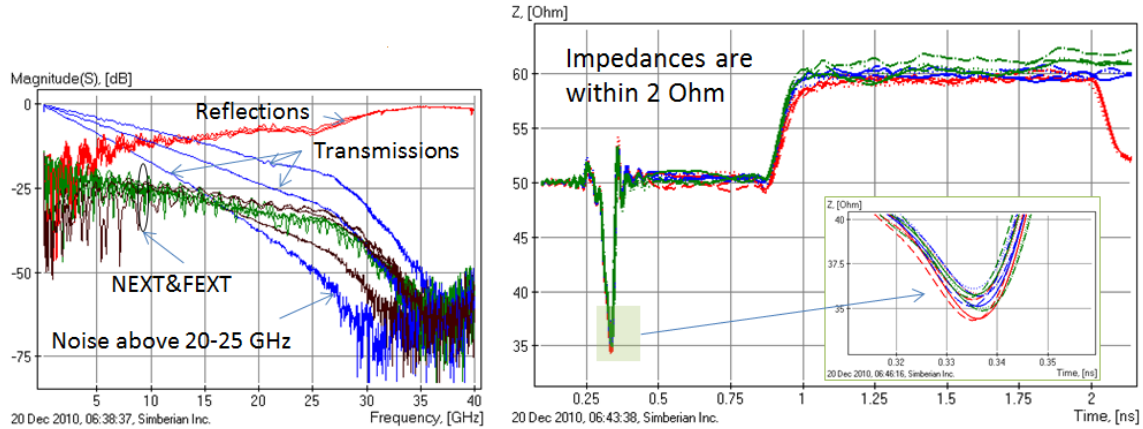


Fig. A.2. Measured single-ended S -parameters for 3 test fixtures with coupled strip line segments (left graph); TDR profile for all coupled strip line structures (right graph, computed with rational macro-model of S -parameters).

With non-identities up to 2-3 Ohm in the impedance profile, we cannot expect high quality of the extracted GMS-parameters. Extracted GMS-parameters are shown in Fig. A.3 for microstrip segments and in Fig. A.4 for strip-line segments. We can observe substantial noise in the insertion loss starting from 15-20 GHz. Group delays are noisy starting from 10 GHz. Note, that the direct polynomial fitting of the GMS-parameters as described earlier did not work in this particular case probably due to variations in width of the actual strips on the board or due to differences in orientation of the traces relative to the glass fibers. The reasons have to be further investigated. **Though, the data are still usable for the meaningful identification of the dielectric properties because of the established trust in the electromagnetic models used to compute the GMS-parameters of the line segments.**

Differences in the modal insertion losses are clearly visible on the measured GMS-parameters for both microstrip and strip-line segments. Even (common) and odd (differential) mode group delays are also different for the coupled microstrip line segment, and almost the same for the strip line segment. Though, modal group delay difference becomes visible for longer line segments that indicate the strip line dielectric inhomogeneity. We can match the insertion loss and group delay at the frequencies below the noise onset, and the model essentially extrapolates the data into higher “noisy” frequencies. The results of such matching are shown in Fig. A.5 for microstrip line segments and in Fig. A.6 for strip line segments. Wideband Debye model [5] was used for all dielectrics here and defined with one frequency point at 1 GHz. Solder mask parameters were left as specified by manufacturer: $DK=4.5$ and $LT=0.02$ (though it does not look right because of it is epoxy and dielectric constant should be smaller). Prepreg parameters have been adjusted to $DK=4.3$ and $LT=0.025$ to match modes for single-ended microstrip lines and for both even and odd modes for the coupled line segments. After the prepreg, the core dielectric parameters have been adjusted to $DK=4.45$ and $LT=0.015$ to match modal parameters for single-ended strip lines as well as for the even and odd modes of the coupled strip line segments. RMS roughness is 0.5 μm and roughness factor is 2.

We have observed that dielectric parameters that produces good match for GMS-parameters extracted from one pair of test fixture may produce not so perfect match for the line segment parameters extracted with another pair of test fixtures. Theoretically they have to be identical, but practically all structures have different defects and in addition the test fixtures with the shorter line segments have different orientation relatively to the dielectric fibers (different effective dielectric constant and impedance on TDR profiles in Fig. A.1 and Fig. A.2). Another source of discrepancies is the ambiguity in the identification of two dielectrics simultaneously. As the result we can observe small differences in behavior of computed and measured modal parameters.

Finally, Table A.1 shows dielectric parameters we have started with and possible values identified with the GMS-parameters. Final dielectric models are causal and frequency-continuous wideband Debye models suitable for simulation of the structures on the board up to 50-100 GHz.

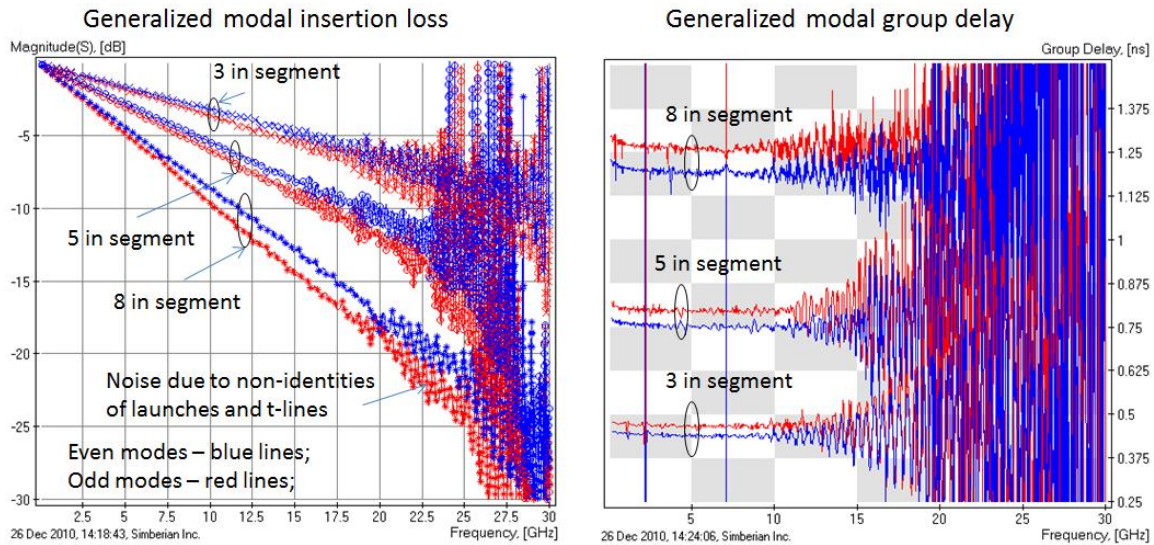


Fig. A.3. Measured GMS-parameters of microstrip line segments extracted from regular S-parameters of 3 in, 6 in and 8 in test fixtures.

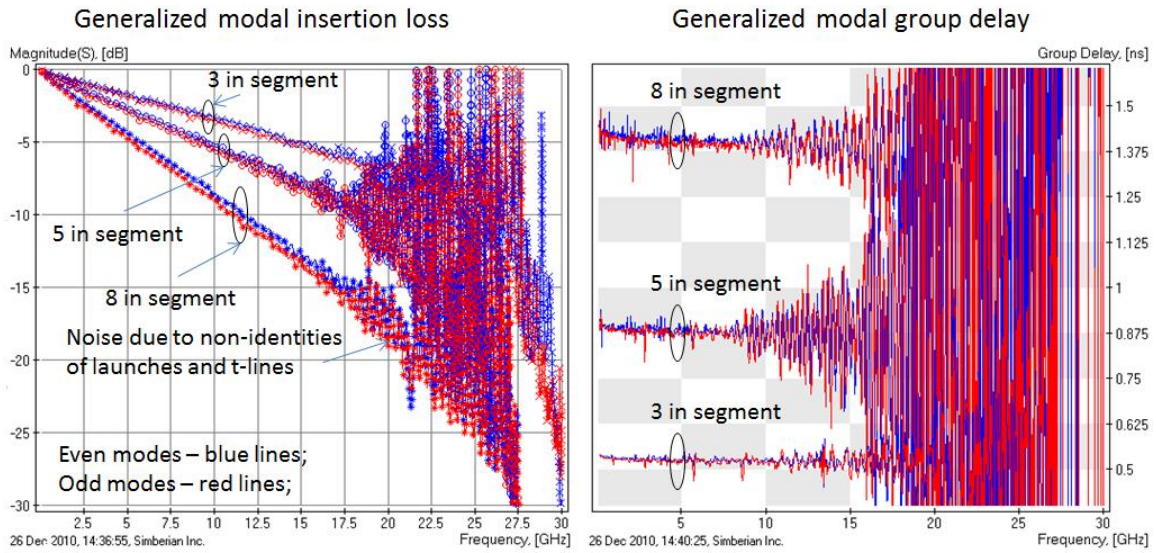


Fig. A.4. Measured GMS-parameters of strip line segments extracted from regular S-parameters of 3 in, 6 in and 8 in test fixtures.

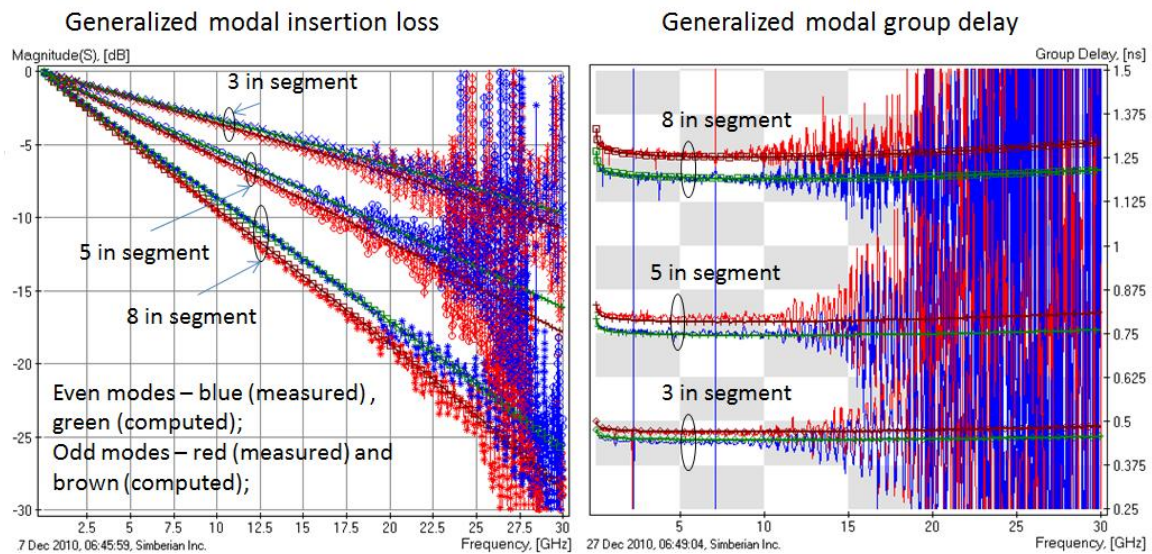


Fig. A.5. Matching measured and computed GMS-parameters of microstrip line segments.

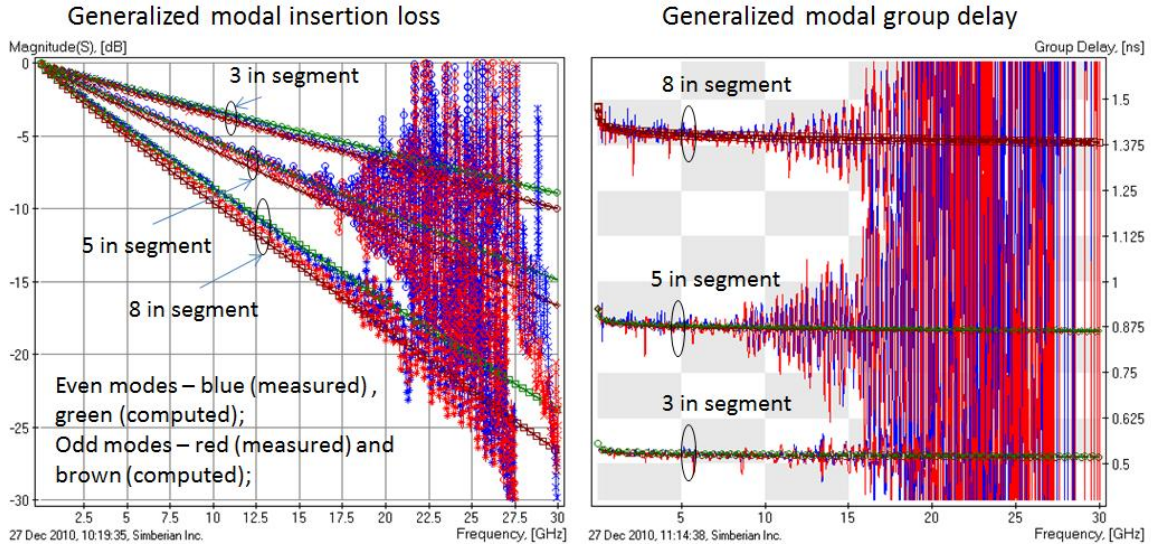


Fig. A.6. Matching measured and computed GMS-parameters of strip line segments.

Table A.1

From manufacturer	DK	LT	Frequency	Notes
Soldermask	4.5	0.02	not specified	
Prepreg	3.8	0.02	not specified	
Core	4.14	0.02	not specified	
Identified				
Soldermask 1	4.5	0.02	1 GHz	
Prepreg 1	4.3	0.025	1 GHz	
Core 1	4.45	0.015	1 GHz	
Soldemask 2	----	----	---	
Prepreg 2	4.2	0.019	1 GHz	Strip only
Core 2	4.5	0.017	1 GHz	Strip only

Appendix B: Oscilloscope Images

3 inch Differential Stripline Comparison of Eye Diagrams
(all are 10Gb/s data streams)

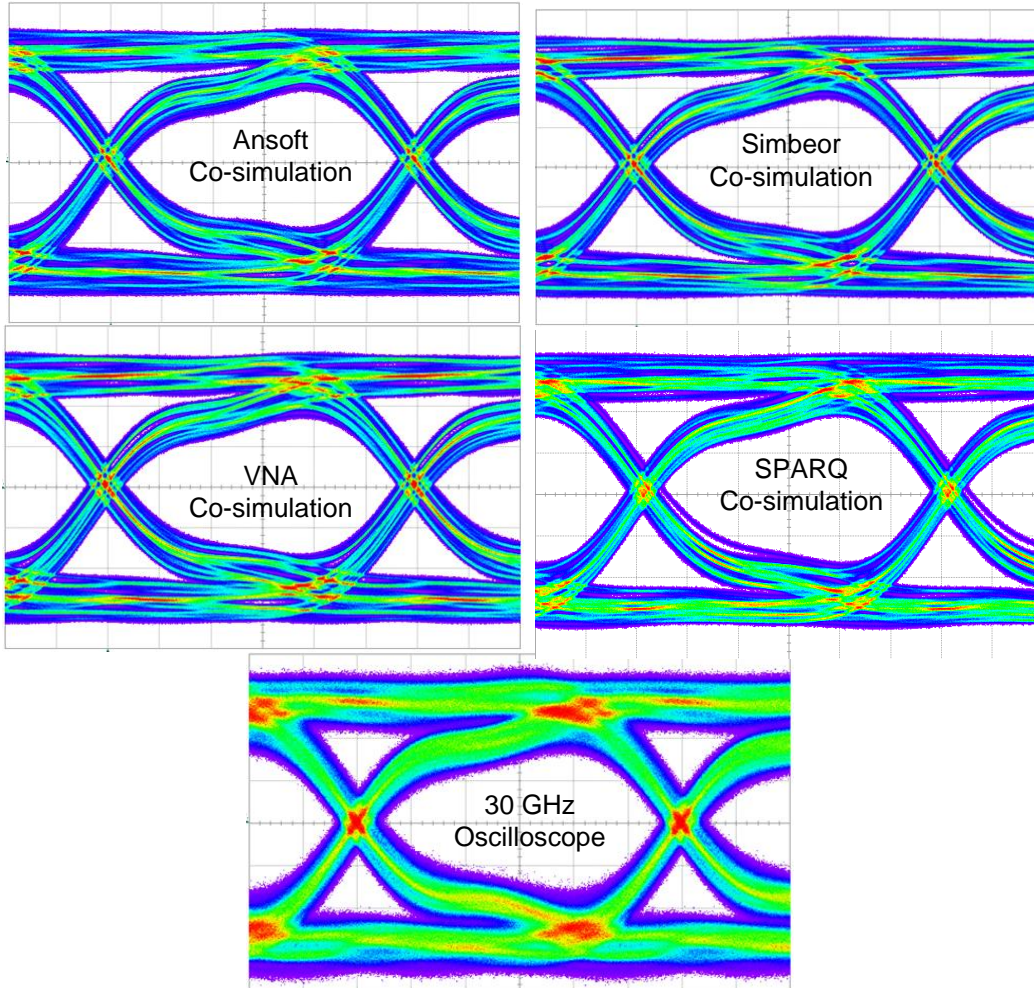


Figure B1: For visual comparison of eye diagrams predicted with Co-simulation (real input stimulus) with emulated “channel”, and last a measure eye-diagram

6 inch Differential Stripline Comparison of Eye Diagrams (all are 10Gb/s data streams)

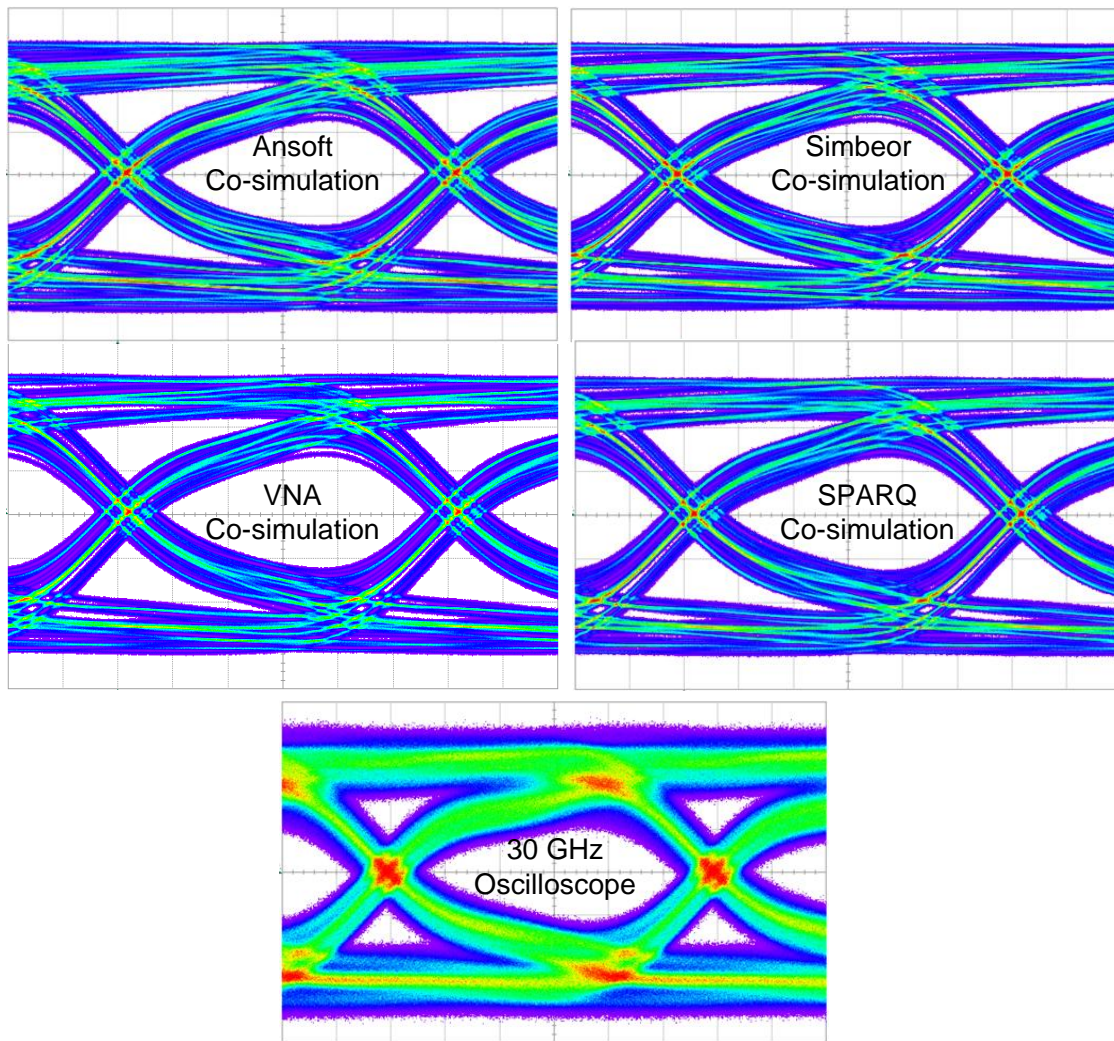


Figure B2: 4 co-simulations and one direct oscilloscope measurement for the 6-inch differential stripline.

11 inch Differential Stripline Comparison of Eye Diagrams (all are 10Gb/s data streams)

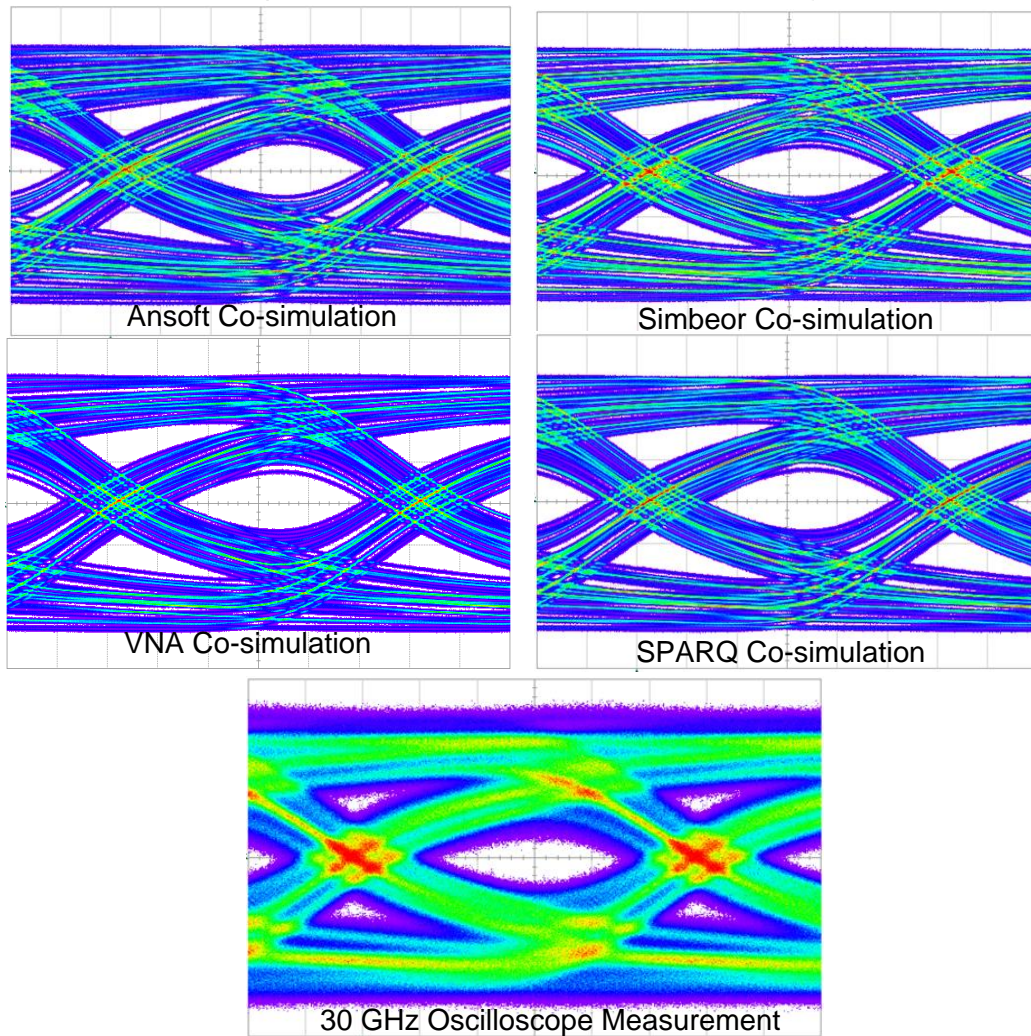


Figure B3: 4 co-simulations and one direct oscilloscope measurement for the 11-inch differential stripline.

References

1. Y. Shlepnev, A. Neves, T. Dagostino, S. McMorrow, Measurement-Assisted Electromagnetic Extraction of Interconnect Parameters on Low-Cost FR-4 boards for 6-20 Gb/sec Applications, DesignCon2009, <http://www.designcon.com/infovault/>
 2. Y. Shlepnev, A. Neves, T. Dagostino, S. McMorrow, Practical identification of dispersive dielectric models with generalized modal S-parameters for analysis of interconnects in 6-100 Gb/s applications, DesignCon2010, <http://www.designcon.com/infovault/>
 3. Simbeor 2011 Electromagnetic Signal Integrity Software, www.simberian.com
 4. Seguinot et al.: Multimode TRL – A new concept in microwave measurements, IEEE Trans. on MTT, vol. 46, 1998, N 5, p. 536-542.
 5. Djordjevic, R.M. Biljic, V.D. Likar-Smiljanic, T.K.Sarkar, Wideband frequency domain characterization of FR-4 and time-domain causality, IEEE Trans. on EMC, vol. 43, N4, 2001, p. 662-667.
 6. Sensitivity of PCB Material Identification with GMS-Parameters to Variations in Test Fixtures, Simberian App Note #2010_03, available at <http://simberian.com/AppNotes.php>
 7. Martin Miller, Michael Schneckner, Quantifying Crosstalk induced Jitter in Multi-lane Serial Data Systems, DesignCon 2009.
 8. Martin Miller, Michael Schneckner, A comparison of Methods for Estimating Total Jitter Concerning Precision, Accuracy and Robustness, DesignCon 2007.
-